

Mapping gene transcription and neurocognition across human neocortex

Justine Y. Hansen¹, Ross D. Markello¹, Jacob W. Vogel², Jakob Seidlitz³, Danilo Bzdok^{1,4,5}, Bratislav Misic^{1*}

¹McConnell Brain Imaging Centre, Montréal Neurological Institute, McGill University, Montréal, Canada

²Department of Psychiatry, Perelman School of Medicine, University of Pennsylvania, PA, USA

³Children's Hospital of Philadelphia and University of Pennsylvania, PA, USA

⁴Biological and Biomedical Engineering, McGill University, Montréal, Canada

⁵Mila, Quebec Artificial Intelligence Institute, Montreal, Canada

Regulation of gene expression drives protein interactions that govern synaptic wiring and neuronal activity. The resulting coordinated activity among neuronal populations supports complex psychological processes, yet how gene expression shapes cognition and emotion remains unknown. Here we directly bridge the microscale and macroscale by mapping gene expression patterns to functional activation patterns across the cortical sheet. Applying unsupervised learning to the Allen Human Brain Atlas and Neurosynth databases, we identify a ventromedial-dorsolateral gradient of gene assemblies that separate affective and perceptual domains. This topographic molecular-psychological signature reflects the hierarchical organization of the neocortex, including systematic variations in cell type, myeloarchitecture, laminar differentiation, and intrinsic network affiliation. In addition, this molecular-psychological signature strengthens over neurodevelopment and can be replicated in two independent repositories. Collectively, our results reveal spatially covarying transcriptomic and cognitive architectures, highlighting the influence that molecular mechanisms exert on psychological processes.

INTRODUCTION

The human brain is an integrated system, involving interactions across multiple scales¹. At the molecular level, fluctuations in gene expression and protein synthesis in neurons drive single-cell activity^{2,3}. The waxing and waning of cellular activity promotes synaptic remodeling^{4,5}, shaping the wiring of nested and increasingly polyfunctional neural circuits^{6,7}. Anatomical connections among mesoscopic neuronal populations promote functional interactions⁸, manifesting as patterned neural activity that drives psychological processes^{9,10}. The regulation of gene expression is therefore naturally intertwined with the brain's structure and function^{11–15}. How molecular dynamics map onto mental states remains a key question in neuroscience.

Modern technological and analytic advances, in concert with global data-sharing initiatives, have created fundamentally new opportunities to link molecular dynamics and psychological processes. High-resolution functional neuroimaging has informed comprehensive meta-analytic atlases of how brain areas selectively respond over a spectrum of perceptual, cognitive and affective experimental manipulations^{16–19}. At the same time, high-throughput microarray profiling has yielded precise genome-wide maps of transcript distributions over the brain^{20–22}, allowing inferences about the spatial distribution of cellular processes and types^{11–13,23–27}. Altogether, the concurrent emergence of global functional genomic and brain mapping initiatives offers an unprecedented chance to identify spatial correspondences between the brain's genetic and cognitive architectures.

Here we directly relate microscale molecular processes to the macroscale functional architecture of the human

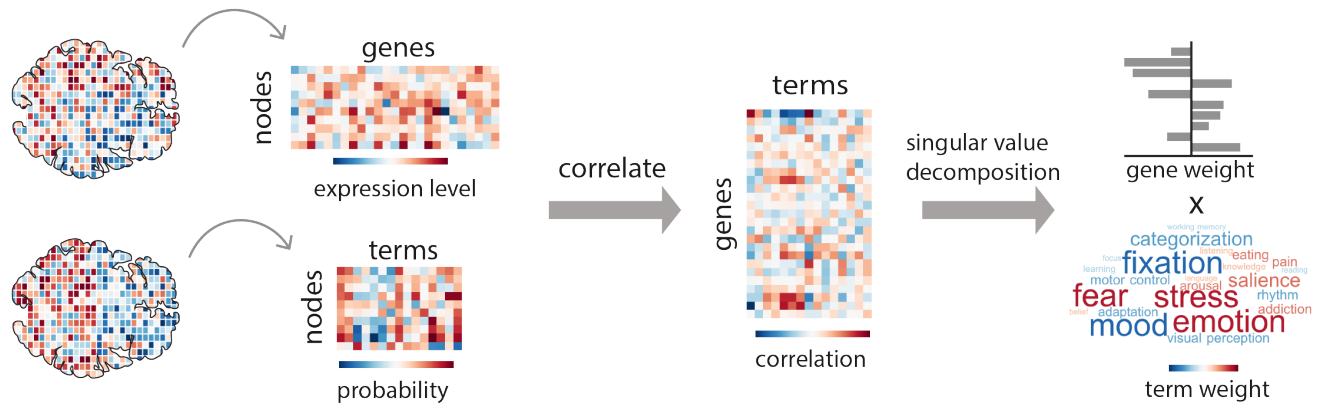
brain. We apply partial least squares analysis to gene expression maps (Allen Human Brain Atlas;²⁰) and probabilistic functional association maps (Neurosynth;¹⁶) to identify molecular signatures related to psychological processes (for a conceptually similar approach, see²⁸). We reveal distinct sets of functionally interrelated genes that span a gradient of psychological processes, and show that this molecular signature corresponds to systematic variation in cell type composition, microstructure, and large scale functional system affiliation. Finally, we perform extensive cross-validation, sensitivity testing and robustness analysis using two independent datasets (BrainMap;¹⁷, and BrainSpan;²²).

RESULTS

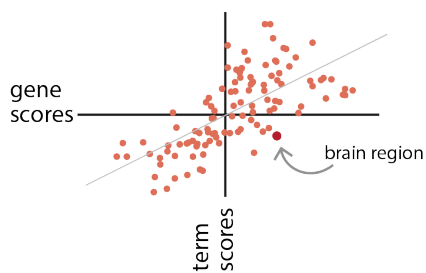
To establish a relationship between gene expression and functional activity, we used the Allen Human Brain Atlas for estimates of gene expression in the brain²⁰, and Neurosynth for probabilistic measures that specific terms (such as “attention”, “emotion”, and “sleep”) are functionally related to specific brain regions¹⁶. This probability, which we call “functional associations”, describes how often specific terms and voxel coordinates are published in conjunction with one another. To facilitate comparison with other reports, only genes with a differential stability greater than 0.1 were retained for analysis (see *Methods*;^{21,26}), and the term set was restricted to those in the intersection of terms reported in Neurosynth and in the Cognitive Atlas³⁰. Gene expression data and probabilistic measures were parcellated into 111 left hemisphere cortical regions of interest^{31,32}. The resulting gene expression matrix was composed of normalized expression levels of 8825 stable genes across 111 target brain regions³², and the functional association matrix represented the functional relatedness of 123 terms to

* bratislav.misic@mcgill.ca

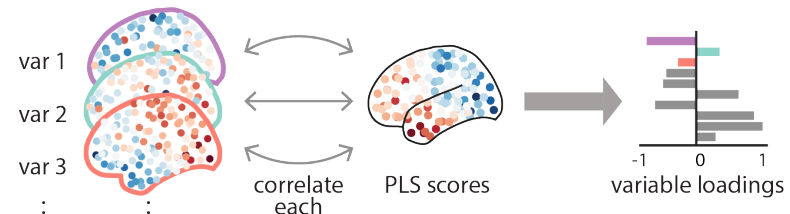
a | partial least squares analysis



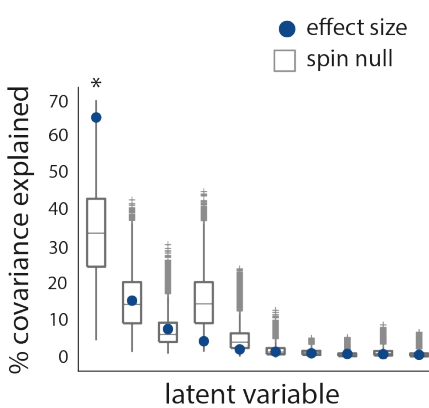
b | scores (projections)



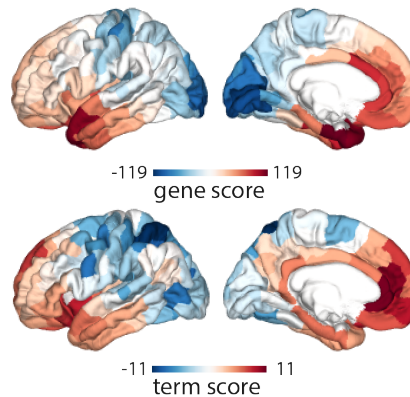
c | loadings



d | effect size



e | score distribution



f | cross-validation

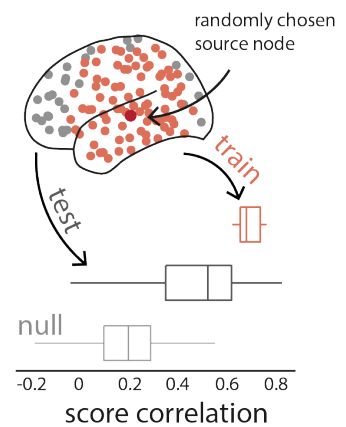


Figure 1. Relating gene expression to functional association | Partial least squares analysis (PLS) was used to identify spatially covarying patterns of gene expression (Allen Human Brain Atlas) and functional association (Neurosynth). (a) PLS relates two data domains by correlating the variables across brain regions and subjecting this to singular value decomposition. This results in multiple latent variables: linear weighted combinations of the original variables (gene weights and term weights) that maximally covary with each other. (b) Gene (term) scores are defined as the product or projection of the original gene expression (functional association) matrix onto the gene (term) weights, such that each brain region is associated with a gene and term score. By design, gene and term scores correlate highly. (c) Gene (term) loadings are defined as the Pearson's correlation between each gene's expression (term's functional associations) across brain regions and the PLS-derived score pattern. (d) Latent variables are ordered according to effect size (the proportion of covariance explained between gene expression and functional association they account for) and shown in blue dots. Statistical significance is assessed with respect to spatial autocorrelation-preserving null model²⁹, shown in grey (10 000 repetitions). Only the first latent variable was statistically significant, accounting for 65% of the covariance between gene expression and functional associations ($p_{\text{spin}} = 0.0228$, bootstrap-estimated 95% CI = [50, 70]). (e) Projecting the original data back onto the PLS-defined gene/term weights results in gene/term scores for each brain region, indexing the extent to which a brain region expresses covarying gene/term patterns. (f) The correlation between gene scores and term scores was cross-validated by constructing the training set with 75% of brain regions closest in Euclidean distance to a randomly chosen source node (red), and the testing set as the remaining 25% of brain regions (dark grey; 100 repetitions). The out-of-sample mean was significant against a permuted null model ($r(26) = 0.4770$, $p_{\text{spin}} = 0.0420$, bootstrap-estimated 95% CI = [0.43, 0.52], 1 000 repetitions, null model shown in light grey). See Supplementary Figure 3 for a comparison with completely random splits. Boxplots in (d) and (f) represent the 1st, 2nd (median) and 3rd quartiles, whiskers represent the non-outlier end-points of the distribution, and crosses represent outliers.

the same 111 brain regions (see Supplementary Table 1 for a full list of terms).

Molecular signatures of psychological processes

We related gene expression to functional associations using partial least squares analysis (PLS), a multivariate statistical technique that extracts optimally covarying patterns from two data domains^{33–35} (Fig. 1a; for results when using canonical correlation analysis (CCA) instead, see Supplementary Figure 1). PLS analysis revealed a single statistically significant latent variable relating gene expression to corresponding functional association across the brain ($p_{\text{spin}} = 0.0228$, bootstrap-estimated CI = [50, 70], one-tailed), where significance was assessed using a permutation test that preserves spatial autocorrelation (“spin test”)^{36,37}. The spin test embodies the null hypothesis that genes and terms are spatially correlated with each other because of inherent spatial autocorrelation. Note that the p-value does not index the contribution of individual terms or genes to the multivariate pattern; this is assessed by bootstrap resampling (see *Methods*). This latent variable represents a pattern of gene expression (gene weights) and a pattern of functional association (term weights), that together capture 65% of the covariance between gene expression and functional association (Fig. 1d; for the PCA decompositions of the individual data matrices, see Supplementary Figure 2). Projecting the gene expression and functional association matrices back onto the gene weights and term weights, respectively, reflects how well a brain area exhibits the gene and term pattern, which we refer to as “gene scores” and “term scores” (Fig. 1b,e). These projections also indicate covariation patterns of gene expression and functional associations. Genes and terms whose activity correlate positively with the score pattern covary with one another in the positively scored regions, and vice versa for negatively scored regions. The pattern of gene and term scores across the brain revealed a dorsolateral to ventromedial gradient, in which dorsolateral regions were scored more negatively and ventromedial regions more positively.

We next cross-validated the correlation between gene and term scores. Due to inherent spatial autocorrelation, proximal regions exhibit similar gene expression profiles and functional activity^{38,39}. Thus, randomly dividing brain regions into training and testing sets may result in interdependencies between the two sets (Supplementary Figure 3). To ensure that the correlation between gene and term scores is not inflated due to spatial autocorrelation, we selected the 75% of brain regions closest in Euclidean distance to a randomly chosen source node as the training set, and the remaining 25% of brain regions as the testing set. This procedure was repeated 100 times and a distribution of Pearson’s correlations for the training and testing set is shown in Fig. 1f. The mean out-of-sample Pearson’s correlation between

gene and term scores was $r(26) = 0.4770$ ($p_{\text{spin}} = 0.0420$, bootstrap-estimated 95% CI = [0.43, 0.52]).

A genomic signature of cognitive processes

The significance of the first latent variable and the cross-validation of score correlations demonstrates there is a relationship between gene expression and functional association. The relationship itself is determined by the terms and genes that contribute most to the latent variable. The loading of each term was computed as the Pearson’s correlation between the term’s functional association across brain regions with the PLS-estimated scores (Fig. 1c). Loadings reflect the shared variance between original variables and the PLS score pattern, and can therefore be interpreted as indexing the degree of contribution of each variable to the PLS-defined latent variable. The 25% most positively and negatively correlated terms were retained as terms that most contribute to the latent variable (Fig. 2a; for the loadings of all reliable terms, see Supplementary Figure 4). Terms with large positive loadings were related to affective processes, including emotion, stress, fear, anxiety, and mood. Terms with large negative loadings were related to perceptual and attentional processes. Examples include attention (of which “visual attention”, “spatial attention”, and simply “attention” were all weighed very highly), visual perception, and imagery. This latent variable thus represents a putative perceptual-affective gradient of functional associations. Note that while negatively scored brain regions are dominant in sensorimotor regions, terms related to attention and perception consistently score higher than sensorimotor terms such as “multisensory” and “coordination”. Moreover, although the spatial pattern involves prominent contribution from both visual and somatomotor cortex, the ranking of Neurosynth terms emphasizes psychological processes associated with simultaneous activation in both; hence, terms associated with perception and attention are ranked higher than terms associated with sensory-motor function per se.

Gene contribution was analogously assessed by computing spatial correlations (loadings) between an individual gene’s expression pattern and the PLS-derived scores (Fig. 1c). Genes were segregated based on the sign of their loadings, where “positive genes” refer to genes with positive loading, and “negative genes” those with negative loading. Strongly contributing genes were defined as those among the top 50% of their respective positive/negative gene set, resulting in 2544 strongly contributing positive genes and 1869 strongly contributing negative genes. The pattern of positive genes covarying with affective terms is strongest in positively scored brain regions (Fig. 2a), and the pattern of negative genes covarying with perceptual terms is strongest in negatively scored brain regions (Fig. 2b).

To better understand the biological significance of the

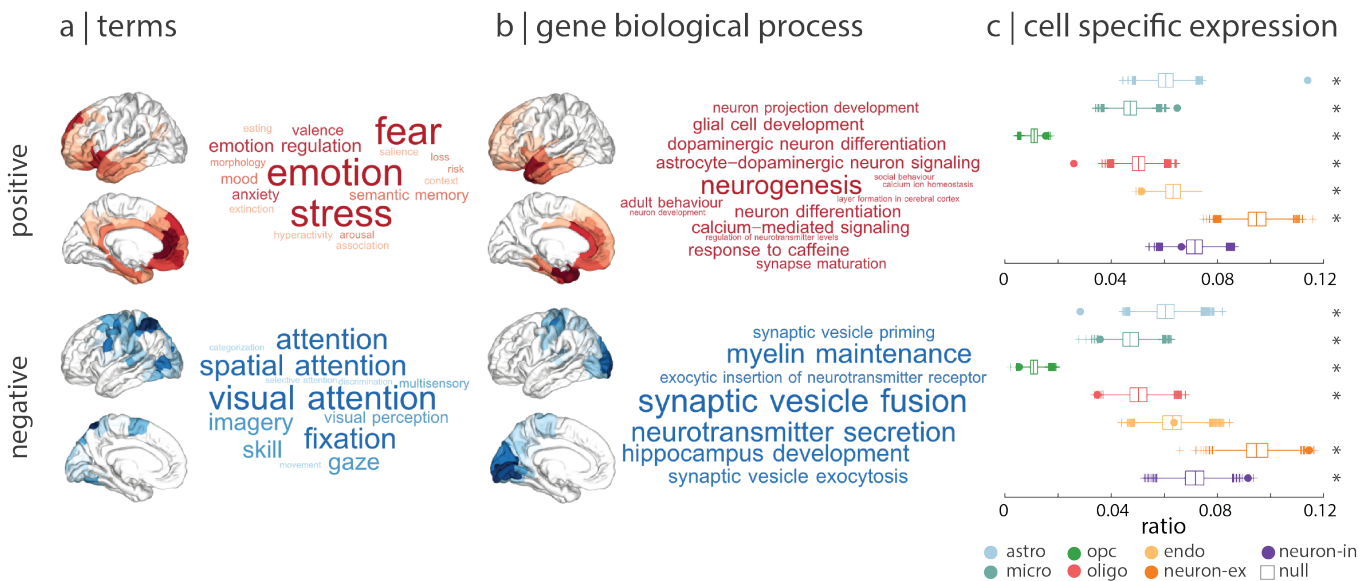


Figure 2. Gene sets underlying psychological processes | Genes and terms that contribute most to the latent variable were analyzed further. (a) The contribution of positively- and negatively-weighted ontological terms to the latent variable were estimated with term loadings: Pearson's correlations between a term's functional association across brain regions and the PLS-derived score pattern. The 25% most positively (red) and negatively (blue) correlated terms reveal a perceptual-affective gradient. Word size represents the relative size of the term loading. (b) Gene contribution was estimated with gene loadings: Pearson's correlations between a gene's expression across brain regions and the PLS-derived score pattern. Biological processes in which the top 50% of genes with positive and negative loading are most involved were identified using Gene Set Enrichment Analysis (see *Methods*) and tested against a spatial autocorrelation-preserving null model³⁹. (c) Cell-type deconvolution was used to identify cell type enrichment in the gene sets identified by PLS²³. The ratio of genes in each gene set preferentially expressed in seven distinct cell types is shown against a null model of a random selection of all genes (boxplots, 10 000 repetitions). Boxplots represent the 1st, 2nd (median) and 3rd quartiles, whiskers represent the non-outlier end-points of the null distribution, and crosses represent outliers. Cell types: ASTRO = astrocyte, MICRO = microglia, OPC = oligodendrocyte precursor, OLIGO = oligodendrocyte, ENDO = endothelial, NEURO-EX = excitatory neurons, NEURO-IN = inhibitory neurons, NULL = empirically derived null distribution.

positive and negative gene sets, we adapted analyses from the Gene Set Enrichment Analysis toolbox (<https://github.com/benfulcher/GeneSetEnrichmentAnalysis>³⁹). We explored the biological processes with which the reliable positive and negative genes are significantly involved (see *Methods* for details and Supplementary Tables 4 and 5 for a full machine-readable list of biological processes and respective *p*-values). A selection of the significant categories most related to brain structure and function are visualized as word clouds in Fig. 2b. In general, affect-related gene sets show enrichment for processes related to neurogenesis and differentiation, while perception-related gene sets are enriched for processes related to synaptic signaling.

Alongside biological process, we asked whether psychologically-relevant genes are preferentially expressed in specific cell types (Fig. 2c). Cell-type deconvolution was performed using cell-specific aggregate gene sets across five human adult postmortem single-cell and single-nucleus RNA sequencing studies^{43–48}, as presented previously (Supplementary Table 5 from²³). Specifically, we calculated the ratio of genes in each gene set preferentially expressed in one of seven cell types: astrocytes, microglia, oligodendrocyte precursors, oligodendrocytes,

endothelial cells, excitatory neurons, and inhibitory neurons (Fig. 2c). Gene sets were thresholded to include the top 50% of genes with greatest loadings (note that although the threshold is arbitrary, the results are highly consistent across a range of thresholds, from 2.5% to no threshold; Supplementary Figure 6). Statistical significance was assessed against a null distribution of ratios constructed by repeating the process 10 000 times on a set of random genes (two-tailed, FDR-corrected). Dominant positive genes (related to affect) are significantly more expressed in astrocytes ($p = 2.3 \times 10^{-4}$), microglia ($p = 2.3 \times 10^{-4}$), and oligodendrocyte precursors ($p = 0.0160$), and significantly less expressed in excitatory neurons ($p = 0.0052$), oligodendrocytes ($p = 2.3 \times 10^{-4}$), and endothelial cells ($p = 0.0052$). Dominant negative genes (related to perception) are significantly more expressed in excitatory neurons ($p = 0.0023$) and inhibitory neurons ($p = 0.0017$), and significantly less expressed in astrocytes ($p < 0.001$), microglia ($p = 0.0114$), oligodendrocytes ($p = 0.0019$) and oligodendrocyte precursors ($p = 0.0114$). Broadly, we find evidence that areas associated with affect are enriched for genetic signal of cells involved in neuron support (astrocytes, microglia); areas associated with perception are enriched for genetic

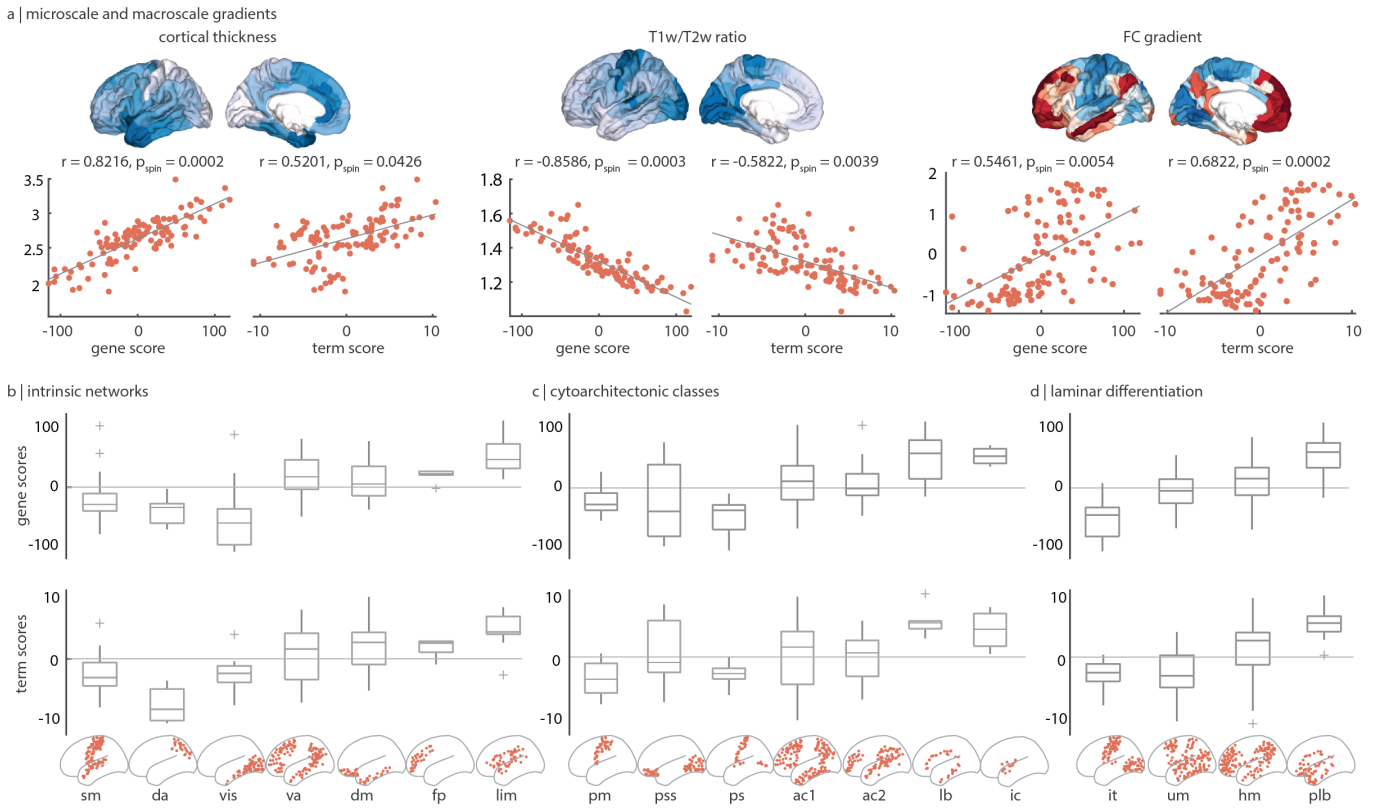


Figure 3. The gene expression-functional association gradient is organized around microscale and macroscale hierarchies

| (a) PLS-derived score patterns are positively correlated with cortical thickness, negatively correlated with intracortical myelin (measured by T1w/T2w ratio), and positively correlated with the principal gradient of functional connectivity (Pearson's r , $n = 111$ brain regions). (b) Distribution of scores across seven intrinsic resting-state functional networks defined by Yeo and colleagues⁹. (c) Distribution of scores across the seven Von Economo cytoarchitectonic classes^{15,40}. (d) Distribution of PLS-derived gene and term scores across the four Mesulam levels of laminar differentiation^{41,42}. Boxplots in (b)–(d) represent the 1st, 2nd (median) and 3rd quartiles, whiskers represent the non-outlier end-points of the distribution, and crosses represent outliers. Network assignments: SM = somatomotor ($n = 23$ regions), DA = dorsal attention ($n = 7$), VIS = visual ($n = 15$), VA = ventral attention ($n = 14$), DM = default mode ($n = 33$), FP = fronto-parietal ($n = 6$), LIM = limbic ($n = 13$), PM = primary motor cortex ($n = 10$), PSS = primary/secondary sensory cortex ($n = 17$), PS = primary sensory cortex ($n = 9$), AC1, AC2 = association cortex ($n = 40, 24$), LB = limbic regions ($n = 7$), IC = insular cortex ($n = 4$), IT = idiotypic ($n = 23$), UM = unimodal ($n = 33$), HM = heteromodal ($n = 37$), PLB = paralimbic ($n = 18$).

signal of neurons themselves (inhibitory and excitatory). This dichotomy also matches the intuition derived from biological process enrichment analysis (Fig. 2b).

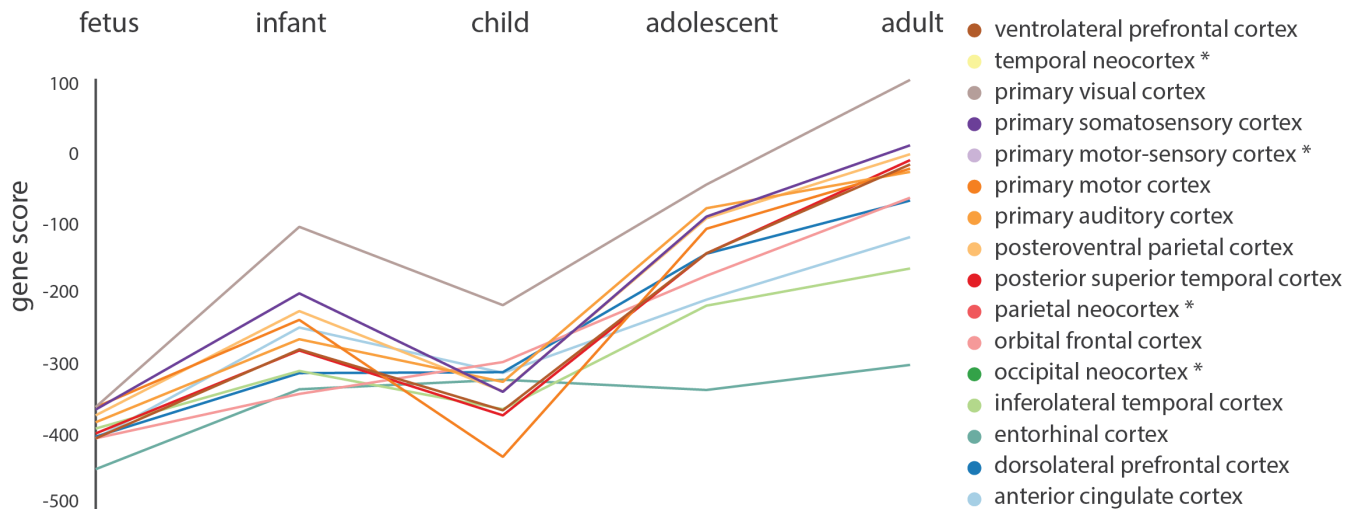
The gene-cognition gradient reflects cortical hierarchies

Having identified a gradient of covarying gene expression and functional association, we next investigated whether these topographic patterns reflect variation in other microstructural and functional attributes^{49,50}. To address this question, we averaged measures of cortical thickness and T1w/T2w ratios (a widely used proxy for intracortical myelin;⁵¹) from the left hemisphere cortex across 417 unrelated subjects from the Human Connectome Project (see Methods). We then computed Pearson's correlations of mean cortical thickness and T1w/T2w

maps with gene score and term score maps (Fig. 3a). We find a strong positive correlation between cortical thickness and PLS scores ($r(109) = 0.82, p_{\text{spin}} < 0.001$, bootstrap 95% CI = [0.75, 0.88] for gene scores, $r(109) = 0.52, p_{\text{spin}} = 0.0426$, bootstrap 95% CI = [0.40, 0.62] for term scores, two-tailed), and a strong negative correlation between T1w/T2w ratio and PLS scores ($r(109) = -0.86, p_{\text{spin}} < 0.001$, bootstrap 95% CI = [-0.90, -0.81] for gene scores, $r(109) = -0.58, p_{\text{spin}} = 0.0039$, bootstrap 95% CI = [-0.67, -0.46] for term scores, two-tailed). Altogether, the gene-association gradient mirrors microstructural attributes^{13,26,52,53}.

Given that the score pattern resembles the differentiation between unimodal and transmodal cortex^{54,55}, we sought to relate the score pattern to the principal functional gradient reported by Margulies and colleagues⁵⁶. For this purpose, we applied diffusion map embed-

a | gene scores across development



b | score correlation

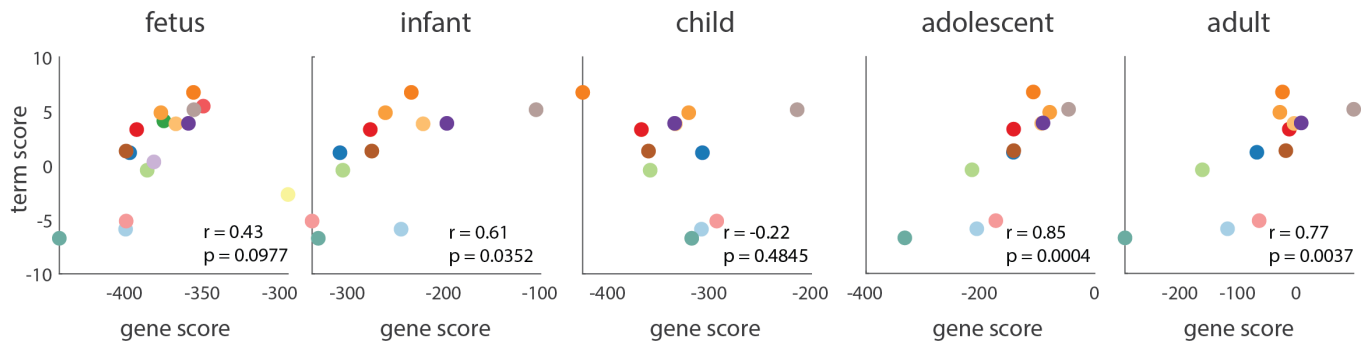


Figure 4. Molecular signature of psychological function strengthens with development | The BrainSpan database was used to replicate the results and also to compare how the isolated genetic signature develops over the lifespan²². (a) Gene scores for twelve unique brain regions gradually increase with development and peak in adulthood. Brain regions with gene expression levels only available in the fetal stage are indicated with an asterisk, and no corresponding curve is shown. (b) The Pearson's correlation between estimated gene scores and PLS-derived term scores is strongest in adolescence and adulthood ($n = 16$ brain regions in the fetus, $n = 12$ regions in all other developmental stages.)

ding on a group-averaged functional connectivity matrix computed from the 1 003 HCP subjects with complete resting-state fMRI data, and extracted the first principal gradient^{57,58}. This gradient situates brain regions on a continuous axis from unimodal primary sensory and motor cortex to transmodal higher association cortex (Fig. 3a). We find that the gene score and term score patterns significantly correlate with this gradient ($r(109) = 0.55$, $p_{\text{spin}} = 0.0054$, bootstrap 95% CI = [0.38, 0.65] for gene scores, $r(109) = 0.68$, $p_{\text{spin}} < 0.001$, bootstrap 95% CI = [0.58, 0.75] for term score, two-tailed; Fig. 3a). This implies that negatively scored regions tend to be more closely aligned with unimodal cortex and positively scored regions tend to be predominantly aligned transmodal cortex.

As a final step, we sought to understand how well

the gene and term score maps conform to other major structural and functional partitions of the human cerebral cortex. We stratified gene and term scores in several complementary ways: (1) within seven intrinsic functional brain networks as defined by Yeo and colleagues⁹, (2) within seven Von Economo classes of cortical cytoarchitecture^{15,40}, and (3) within four Mesulam levels of laminar differentiation across the cortex^{41,42} (Fig. 3b-d). Consistent with the notion that the gene expression-functional association gradient reflects a differentiation between perceptual and affective psychological domains, we observe a separation between limbic/paralimbic and somato-motor/idiotypic networks across all three partitions.

Gene-cognition convergence over development

Given the continuous development of cognitive processes over the lifespan, we sought to track the gene expression-functional association signature through human development. We used BrainSpan, a dataset that provides gene expression estimates from brain tissue samples aged eight post-conception weeks (pcw) to forty years, across sixteen unique cortical regions²². To best replicate the original analyses, genes were selected if they were included in the original list of 20 503 genes from AHBA, and if their differential stability was greater than 0.1, as defined on the 34-node parcellation. A region by gene expression matrix was constructed for five different life stages: fetal, infant, child, adolescent, and adult (see *Methods* for details). Gene scores were estimated as the projection of the BrainSpan-defined gene expression matrices onto the PLS-defined gene weights, yielding an estimated gene score per region and life stage (Fig. 4a). The molecular signature, represented by gene scores, increases with development, suggesting the gene expression-functional association gradient becomes more pronounced with maturation. In other words, the genetic signal captured by the original PLS analysis is specific to adult-derived cells.

We also used the BrainSpan dataset to assess the robustness of the original PLS model. For each life stage, we correlated the 16 estimated gene scores to the PLS-defined term scores, as determined by the 34-node parcellation. To achieve this, we manually defined a region-to-region mapping, defining each of the 34 regions as a child of a region from the 16-node parcellation. We then averaged the term scores across sibling nodes to yield a single term score for each of the 16 BrainSpan-defined cortical regions (Fig. 4b). Estimated gene scores and term scores correlated significantly in the infant ($r(10) = 0.61$, $p = 0.0352$, bootstrap 95% CI = [0.03, 0.83]), adolescent ($r(10) = 0.85$, $p < 0.001$, bootstrap 95% CI = [0.70, 0.96]), and adult ($r(10) = 0.77$, $p = 0.0035$, bootstrap 95% CI = [0.54, 0.95]) life stages.

Sensitivity and robustness analysis

All analyses presented thus far were conducted on a particular parcellation of brain regions and a predefined set of genes. To ensure the observed results are not dependent on these methodological choices, we compared results when analyses were repeated across different node resolutions and gene sets. Furthermore, we replicated the results using a second dataset for the construction of the functional association matrix.

To ascertain our findings against different choices of parcellation resolution, gene expression and functional association matrices were parcellated into three resolutions: a 34-node parcellation, a 57-node parcellation, and a 111-node parcellation³². Importantly, the 57-node and 111-node parcellations are derived by dividing the

34-node parcellation into smaller parcels, such that each node in the 57- and 111-node parcellations is a child of a node in the 34-node parcellation. Furthermore, since the original analyses were conducted on differentially stable genes (see *Methods*), and the calculation of differential stability depends on parcellation resolution, the number of stable genes retained across parcellations varied (between 8 825 and 11 560 genes retained). The gene expression and functional association matrices at these three resolutions were subjected to PLS and the gene scores and term scores were computed. In the two finer resolutions, the mean score of sibling nodes was computed such that one score for each of the 34 parent nodes was available for all three resolutions. Correlating gene scores and term scores across resolutions revealed an almost one-to-one relationship, indicating node resolution has little impact on gene scores and term scores (Supplementary Figure 7).

Likewise, we asked whether the gene sets contributing most to the latent variable would be altered based on which genes were included in the gene expression matrix. Since the two gene sets underlying perception and affect are defined based on gene loadings, we compared loadings of genes across six variations of the gene expression matrix. For each of the three resolutions introduced above, one matrix includes all 20 323 genes and another includes only differentially stable genes, as defined by the specific parcellation. Each of the six gene expression matrices, alongside their corresponding Neurosynth functional association matrix, were subjected to PLS analysis and loadings were computed for each gene, where genes with the top 50% of positive and negative loadings are considered reliable. When compared across the six different gene expression matrices, we find that reliable gene sets are highly consistent (Supplementary Figure 8).

We next replicated original results using a different data source for the construction of the functional association matrix. BrainMap is a manually curated database of published voxel coordinates from neuroimaging studies that are significantly activated or deactivated during tasks^{17,59–61}. Using the analytic pipeline we previously applied to Neurosynth, we converted BrainMap data into a functional association matrix of probabilities, which included 66 terms (see *Methods* for details, and Supplementary Table 2 for a full list of terms).

PLS analysis on the original gene expression matrix with this BrainMap-derived functional association matrix again revealed a single statistically significant latent variable that captured 51% of the covariance between gene expression and functional association ($p_{\text{spin}} = 0.0034$). The gene and term score distributions again follow a ventromedial-dorsolateral gradient (Supplementary Figure 9a), and gene weights were highly correlated with the original Neurosynth-derived gene weights (Supplementary Figure 9b). Term loadings were computed and the reliable positively and negatively correlated terms are shown in Supplementary Figure 9c. Un-

like the terms used in the Neurosynth-derived functional association matrix, some terms in BrainMap were pharmacological in nature. Interestingly, positive pharmacology terms are primarily depressants (like alcohol and marijuana), and negative pharmacology terms are primarily stimulants (like caffeine).

DISCUSSION

In the present report, we identify spatially covarying gradients of gene expression and functional association across the neocortex. Collectively, these patterns delineate a ventromedial-dorsolateral axis, separating gene sets related to perceptual versus affective function. The spatial patterning of gene and term scores follows a hierarchical organization and is closely related to multiple structural and functional attributes. We assess the robustness of our results in two distinct datasets and show that the gene-association signature strengthens with human development. Our results directly bridge microscale gene expression to macroscale functional processes and highlight the influence that molecular mechanisms have on cognition and behaviour.

The present findings build on previous reports that link gene expression to the structural and functional architecture of the brain. Gene expression profiles have been linked to cortical folding⁶², cortical shrinkage during adolescence²⁴, subcortical connectivity⁶³, and patterns of long-distance and short-distance neural communication^{12,15,64}. In particular, intracortical myelin distribution, as measured by T1w/T2w ratio, is correlated with regional transcription levels, potentially reflecting a hierarchical axis of cytological properties, including cytoarchitecture and cell density^{13,26}. Additionally, the extracted gene pattern closely resembles a number of previously-reported transcriptional maps, including the first principal component of gene expression²⁰, and the gene expression maps associated with magnetization transfer²⁴, disease vulnerability²³, structural and functional network topology¹⁵. While these reports demonstrate a link between transcription and multiple structural features, the functional and behavioural manifestation of such trends remains unknown. Our results fill in this critical gap, showing a statistical correspondence between transcription and psychological function, that is likely to be mediated by microstructure. Collectively, the topographic alignment of molecular and structural features appears to reflect a dominant underlying organizational axis, shaping regional functional specialization.

What do the present findings show us about the regional specialization for psychological functions? Although we have summarized the gene-association gradient as one primarily differentiating perceptual and affective processes, greater nuance is warranted. In particular, the posterior/dorsal system is more specifically related to perception, orienting and attention,

whereas the anterior/ventral system is more specifically related to emotion and evaluation. Thus, the axis differentiates attentional and evaluation functions, and may be more aptly termed an “affective-attentive” or “evaluation-perception” axis. Interestingly, many of the intermediate terms that do not load highly on either end of the axis are integrative in nature (e.g. “consciousness”, “integration”, “episodic memory”, “communication”, etc.; Supplementary Figure 4), suggesting that these more complex functions lie at the intersection of the two systems.

How covarying patterns of gene expression and functional association emerge over the course of ontogeny and phylogeny remains an open challenge. Patterns of gene expression are involved in cortical reorganization during neurodevelopment, including folding⁶², pruning²⁴ and establishment of cortico-cortical connectivity²⁵. In the BrainSpan dataset, we find that the gene-cognition signature has a protracted trajectory over development, gradually becoming most prominent in adulthood (Fig. 4). This external confirmation of our results suggests continued refinement and differentiation of perceptual-affective processes during maturation, but more research is necessary to understand the behavioural consequences of this process at the individual participant level. A related question is how the association between transcription and functional activation evolves across phylogeny. In particular, evolutionary expansion of the cortical mantle is thought to have altered the relationship between molecular gradients and microcircuitry, promoting increasingly complex cognitive function^{64,65}. Thus, the present work could be extended by comparing psychologically-relevant expression patterns, biological processes and cell-type composition across species.

Indeed, one possible explanation for the relative ordering of terms in the PLS model could be that processes at the ends of the spectrum, related to affect and perception/attention, are putatively more basal and thus retain a stronger link with gene expression⁶⁵. Recent work on inter-individual differences in resting-state fMRI connectivity is consistent with this notion, with lower inter-individual variability and lower fingerprinting identifiability in somatomotor and visual cortex, and in ventromedial regions^{66,67}, suggesting that activations in these areas may be more readily elicited in experimental settings. At the same time, many of the high-scoring regions in the present PLS model do show considerable (although not maximal) inter-individual variability, particularly medial and dorsolateral prefrontal cortex. How genomic-neurocognitive links vary across individuals is a key question for future studies.

We map whole-genome transcription patterns to a spectrum of psychological functions across multiple brain areas, but the relationship between gene expression and behaviour has been previously approached from different directions. One approach is to focus on a region of interest. For instance, variations in cognitive

function reflect a transcriptional gradient across the long axis of the hippocampus⁶⁸. An alternative approach is to map single functions of interest to single genes or gene modules. For instance, Fox and colleagues used Neurosynth and AHBA to identify multiple gene-cognition associations in subcortex, including previously established associations between dopamine receptor genes and reward functions in the basal ganglia, as well as novel associations²⁸. The results reported here open new possibilities for mapping high-dimensional transcriptional readouts to neurocognitive function in a data-driven and multivariate analysis framework⁶⁹, broadening the scope of inquiry to multiple gene sets and comprehensive neurocognitive profiles.

Mapping transcription to cognition opens a new way to generate top-down hypotheses about genes involved in a specific psychological process, or bottom-up hypotheses about the psychological correlates of specific genes. We envision that these data will motivate future mechanistic studies of transcriptomic vulnerability in disease²³. For instance, modern psychiatry increasingly emphasizes complex multidimensional profiles of individual patients that include diverse aspects of cognitive performance and affect⁷⁰. Thus, to design therapies tailored to the psychological profiles of individual patients, it is necessary to first map gene expression to psychological processes. In addition, the mapping between genes and cognition offers a powerful biological lens that can reveal multiple targets for therapeutic intervention, from single genes, to gene assemblies, to molecular pathways, to cell types.

A salient example of how this mapping can inform and conceptually link previous findings is in the domain of mood disorders. First, our findings show that meta-analytic activation related to emotion/affect is strongly associated with support cells (astrocytes, microglia) rather than neurons. This is consistent with the inflammation hypothesis, which posits that repeated systemic exposure to microglia-mediated inflammation is a significant risk factor for multiple mental illnesses⁷¹. Second, this affect-related genomic signature is centered on the anterior cingulate cortex, which is disproportionately vulnerable in mental illnesses⁷²⁻⁷⁴. Interestingly, this signature is enriched for neurogenesis and differentiation, rather than signaling, suggesting a potential developmental origin of this vulnerability. Altogether, these findings provide the potential to integrate multiple scales of description of mood disorders.

Here, we demonstrate a statistical correspondence between two modalities that are both structurally embedded in the brain. As with any statistical analysis related to biological mechanisms, caution is warranted when interpreting results. We triangulate towards a statistical mapping between gene expression and functional association using conservative null models, cross-validation, external datasets, and across a range of parcellations and gene sets, but each avenue alone does not yield an overwhelmingly strong result. Furthermore, as we discuss

above, the structural architecture of the brain is likely a mediating factor between these modalities. Although we report an association between gene expression and functional association that is statistically unexpected based on autocorrelation alone (65% covariance), autocorrelation may still account for a considerable portion of the covariance explained between both datasets (34% covariance). Future research is required to identify how the structural architecture of the brain ties transcription to psychology, and is needed to demonstrate a clear and causal biological link between these two modalities.

The present work should be understood alongside some important methodological considerations. First, the main analysis involved two singular datasets, potentially limiting the generalizability of the results. Despite extensive robustness analyses, the present findings are based on small samples of post-mortem brains and more comprehensive microarray gene expression datasets are necessary for future studies. Furthermore, replication of results was only conducted on one external dataset at a time and external validation using BrainMap and BrainSpan together could not be done due to the limited number of cortical genetic samples. Second, all analyses were performed in the left cerebral cortices of the six donors, precluding any tests of lateralized brain function, such as language. Third, due to well-documented differences in transcriptional signatures of cortex, subcortex and cerebellum⁷⁵, the present investigation focused only on the cortex. How gene expression and functional coactivation covary in subcortical structures should be investigated in future work²⁸. Fourth, the mapping of functional activation to psychological terms in Neurosynth cannot distinguish activations from deactivations¹⁶. Thus, the present results identify gene assemblies whose expression covaries with functional associations, but do not isolate the direction of effect.

In summary, we demonstrate that patterns of gene expression influence cognition and emotion. Organized across a spatially ordered ventromedial-dorsolateral gradient, we show that this genetic signature shapes the composition of cell types and microstructure, ultimately manifesting as a large-scale axis differentiating affective and perceptual processes. Collectively, these results highlight a statistical link between molecular dynamics and psychological function.

METHODS

Microarray gene expression

Regional microarray expression data were obtained from six post-mortem brains provided by the Allen Human Brain Atlas (<http://human.brain-map.org/>)²⁰. Since only two of the six brains included samples from the right hemisphere, analyses were conducted on the left hemisphere only. All processing was performed using the *abagen* toolbox (<https://github.com/netneurolab/>

abagen). These data were processed and mapped to parcellated brain regions at three increasingly finer resolutions, from 34 to 111 left hemisphere cortical grey matter nodes according to the Lausanne anatomical atlas^{31,32}.

Microarray probes were reannotated using data provided by Arnatkevičiūtė et al.²⁷. A single microarray probe with the highest differential stability, $\Delta_S(p)$, was selected to represent each gene²¹, where differential stability was calculated as:

$$\Delta_S(p) = \frac{1}{\binom{N}{2}} \sum_{i=1}^{N-1} \sum_{j=i+1}^N r[B_i(p), B_j(p)] \quad (1)$$

Here, r is Spearman's rank correlation of the expression of a single probe p across regions in two donor brains, B_i and B_j , and N is the total number of donor brains. This procedure retained 20 232 probes, each representing a unique gene. Note that probe selection can alternatively be achieved using RNA-seq data⁷⁶, which produces highly similar PLS results (gene scores, term scores, and term weights all highly correlated across methodology, $r > 0.99$).

Next, samples were assigned to brain regions using MNI coordinates generated via non-linear registrations (<https://github.com/chrisfilo/alleninf>) by finding the nearest region, up to 2mm away. To reduce the potential for misassignment, sample-to-region matching was constrained by hemisphere and cortical/subcortical divisions²⁷. If a brain region was not assigned any sample based on the above procedure, the sample closest to the centroid of that region was selected in order to ensure that all brain regions were assigned a value.

Inter-subject variation was addressed by normalizing tissue sample expression values for each donor across genes using a scaled robust sigmoid function¹².

$$x_{norm} = \frac{1}{1 + \exp(-\frac{(x_g - \langle x_g \rangle)}{IQR_x})} \quad (2)$$

where $\langle x_g \rangle$ is the median and IQR is the normalized interquartile range of the expression value of a single gene across regions. Normalized gene expression values were then rescaled to a unit interval:

$$x_{scaled} = \frac{x_{norm} - \min(x_{norm})}{\max(x_{norm}) - \min(x_{norm})} \quad (3)$$

Gene expression values were normalized across tissue samples using the same procedure. Samples assigned to the same brain region were then averaged separately for each donor. Scaled regional expression profiles were finally averaged across donors, resulting in a single matrix \mathbf{X} with r rows corresponding to brain regions and g columns corresponding to the retained 20 232 genes. A threshold of 0.1 was imposed on the differential stability of each gene, such that only stable genes were

retained for future analysis. Genes with large differential stability have been previously shown to be related to biological relevance, disease, drug targets, and literature citations²¹. Furthermore, this stability threshold minimizes the influence of unreliable gene expression measurements by preferentially selecting genes whose expression is consistent across the six sampled brains. At the 34-node, 57-node, and 111-node resolutions, the ensuing number of stable genes retained was 11 560, 10 453, and 8 825, respectively.

Term functional associations

Probabilistic measures of the association between voxels and terms were obtained from Neurosynth, a meta-analytic tool that synthesizes results from more than 15 000 published fMRI studies by searching for high-frequency key words (such as “pain” and “attention”) that are published alongside fMRI voxel coordinates (<https://github.com/neurosynth/neurosynth>, using the volumetric association test maps¹⁶). This measure of association is the probability that a given term is reported in the study if there is activation observed at a given voxel. Note that the tool does not distinguish between areas that are activated or deactivated in relation to the term of interest, nor the degree of activation, only that certain brain areas are frequently mentioned in conjunction with certain words. Although more than a thousand terms are reported in Neurosynth, we focus primarily on cognitive function and therefore limit the terms of interest to cognitive and behavioural terms. These terms were selected from the Cognitive Atlas, a public ontology of cognitive science³⁰, which includes a comprehensive list of neurocognitive terms and has been previously used in conjunction with Neurosynth²⁹. We used $t = 123$ terms, ranging from umbrella terms (“attention”, “emotion”) to specific cognitive processes (“visual attention”, “episodic memory”), behaviours (“eating”, “sleep”), and emotional states (“fear”, “anxiety”). The coordinates reported by Neurosynth were parcellated into 111 left-hemisphere cortical regions. The probabilistic measure reported by Neurosynth can be interpreted as a quantitative representation of how regional fluctuations in activity are related to psychological processes. For simplicity, we refer to these probabilities as “functional associations” throughout the present report. The full list of terms is shown in Supplementary Table 1.

Partial least squares analysis

Partial least squares analysis (PLS) was used to relate gene expression to functional association. PLS is an unsupervised multivariate statistical technique that decomposes relationships between two datasets (in our case, gene expression, $\mathbf{X}_{n \times g}$ and functional association, $\mathbf{Y}_{n \times t}$) into orthogonal sets of latent variables with maximum

covariance, which are linear combinations of the original data. This was done by z-scoring both data matrices columnwise and applying singular value decomposition on the matrix $\mathbf{Y}'\mathbf{X}$ such that

$$(\mathbf{Y}'\mathbf{X})' = \mathbf{USV}' \quad (4)$$

where $\mathbf{U}_{g \times t}$ and $\mathbf{V}_{t \times t}$ are orthonormal matrices consisting of left and right singular vectors, and $\mathbf{S}_{t \times t}$ is a diagonal matrix of singular values (Fig. 1a)⁷⁷. The i^{th} columns of \mathbf{U} and \mathbf{V} constitute a latent variable, and the i^{th} singular value in \mathbf{S} represents the covariance between singular vectors. The i^{th} singular value is proportional to the amount of covariance between gene expression and functional association captured by the i^{th} latent variable, where the effect size can be estimated as the ratio of the squared singular value to the sum of all squared singular values. In the present study, the left singular vectors (i.e. the columns of \mathbf{U}) represent the degree to which each gene contributes to the latent variable and demonstrates the extracted association between gene expression and functional associations (“gene weights”; see Supplementary Table 6 for a complete list of gene weights). The right singular vectors (i.e. the columns of \mathbf{V}) represent the degree to which the cognitive terms contribute to the same latent variable (“term weights”). Positively weighed genes covary with positively weighed terms, and negatively weighed genes covary with negatively weighed terms. Gene and term scores at each brain region for each latent variable can be computed by projecting the original data onto the singular vector weights (Fig. 1b,e). Positively scored brain regions are regions that demonstrate the covariance between expression of positively weighted genes and association of positively weighted cognitive terms (and vice versa for negatively scored brain regions):

Gene scores for latent variable $i = \mathbf{X}_{n \times g} \mathbf{U}(i)_{g \times 1}$

Term scores for latent variable $i = \mathbf{Y}_{n \times t} \mathbf{V}(i)_{t \times 1}$.

Loadings for each variable were computed as the Pearson’s correlation between each individual variable’s activity (gene expression and term functional associations) and the PLS-derived gene score pattern (Fig. 1c, Supplementary Figure 4). Note that term loadings could have been alternatively computed as the correlation between an individual term’s functional associations and the PLS-derived term score pattern (Supplementary Figure 5); term loadings are highly correlated between methodology ($r(121) = 0.95$, $p < 0.001$, bootstrap 95% CI = [0.9426, 0.9687]). Squaring the loading (a correlation) equals the percent variance shared between an original variable (a specific gene or term) and the PLS-derived latent variable. Terms and genes with high absolute loading are variables that are highly correlated to the score pattern, indicating a large amount of shared variance between the individual variable and the latent variable.

The reliability of gene and term loadings was assessed using bootstrap resampling (see the following subsection).

Note that, by design, PLS does not pre-whiten the two data matrices prior to the decomposition, such that the model takes into account both within-set and between-set relationships^{78,79}. As a result, the data matrix with the stronger correlation structure may drive the solution. Canonical correlation analysis (CCA) is a similar reduced rank regression that seeks to match two sets of variables by extracting patterns in the original dataset that maximally correlate (instead of covary, as in PLS)⁸⁰. Unlike PLS, CCA removes within-set correlations by pre-whitening the data, thus theoretically eliminating the possibility that the correlation structure in one dataset would dominate the solution. In other words, CCA is designed such that one data domain cannot bias the results away from the other data domain. To investigate whether CCA and PLS would yield different results, we applied CCA to the gene expression and functional association matrices, and find similar results (Supplementary Figure 1).

The robustness of the PLS model was assessed by cross-validating the correlation between gene scores and term scores (Pearson’s r). Since our observations are brain areas and therefore nonindependent, we designed the cross-validation such that the training and testing set were composed of spatially distant brain regions. To achieve this, a random source node and the 75% of brain regions closest in Euclidean distance composed the training set, and the remaining 25% of brain regions composed the testing set (Fig. 1d). PLS was used to compute gene scores and term scores from the training set, as well as the correlation between the two ($\text{Corr}(\mathbf{X}_{\text{train}} \mathbf{U}_{\text{train}}, \mathbf{Y}_{\text{train}} \mathbf{V}_{\text{train}})$). The test set was projected onto the training-derived singular vector weights to generate predicted gene and term scores, and the correlation between predicted scores was computed ($\text{Corr}(\mathbf{X}_{\text{test}} \mathbf{U}_{\text{train}}, \mathbf{Y}_{\text{test}} \mathbf{V}_{\text{train}})$). This procedure was repeated 100 times, yielding a distribution of score correlations for the training and testing sets (Fig. 1d). The significance of the mean out-of-sample correlation was assessed against a permuted null model, constructed by repeating the cross-validation on spatial autocorrelation-preserving permutations of the functional association matrix (1 000 repetitions, Fig. 1f).

Bootstrap resampling

The reliability of the gene (term) weights was assessed using bootstrap resampling. The rows (brain regions) of the gene expression (functional association) matrix were randomly selected with replacement 10 000 times. PLS was recomputed using this new bootstrapped gene expression (functional association) matrix and the original functional association (gene expression) matrix. This was repeated 10 000 times to estimate a sampling dis-

tribution of gene (term) weights. The ratio of the true gene (term) weight to the standard error of its bootstrap resampled distribution (termed “bootstrap ratio”) was computed⁸¹. Genes and terms with large bootstrap ratios have large weights (i.e. contribute greatly to the relationship captured by the latent variable) and have small standard error (i.e. are reliable). Note that bootstrap ratios are highly correlated to gene loadings ($r(8823) = 0.94$, $p < 0.001$, bootstrap 95% CI = [0.9406, 0.9441]).

Null model

Spatial autocorrelation-preserving permutation tests were used to assess statistical significance of associations across brain regions, termed “spin tests”²⁹. We created a surface-based representation of the parcellation on the FreeSurfer fsaverage surface, via files from the Connectome Mapper toolkit (<https://github.com/LTS5/cmp>). We used the spherical projection of the fsaverage surface to define spatial coordinates for each parcel by selecting the coordinates of the vertex closest to the center of the mass of each parcel³⁶. These parcel coordinates were then randomly rotated, and original parcels were reassigned the value of the closest rotated parcel (10 000 repetitions). Parcels for which the medial wall was closest were assigned the value of the next most proximal parcel instead. The procedure was performed at the parcel resolution rather than the vertex resolution to avoid upsampling the data, and only to the left hemisphere.

In PLS analysis, the spin test is applied to the singular values (or equivalently, the covariance explained) of the latent variables, producing a null distribution of singular values. This is done applying PLS analysis to the original gene expression matrix and a spun term association matrix. The spin test embodies the null hypothesis that genes and terms are spatially correlated with each other because of inherent spatial autocorrelation. The p-value is computed as the proportion of null singular values that are greater in magnitude than the empirical singular values. Thus, the p-value represents the probability that the observed spatial correspondence between genes and terms could occur by randomly correlating maps with comparable spatial autocorrelation (Fig. 1d, grey boxplots; normality of the data distributions was not formally tested). P-values for all latent variables can be found in Supplementary Table 3 and examples of null gene and term scores can be found in Supplementary Figure 10.

Gene set analysis

To determine the biological processes in which the gene sets identified by PLS are most involved, we adapted analyses from the Gene Category Enrichment Analysis toolbox (originally available at <https://github.com/benfulcher/GeneCategoryEnrichmentAnalysis>³⁹;

for the original approach, see⁸²). Each biological process category is associated with a subset of genes, annotations of which are provided by the Gene Ontology (geneontology.org). To determine the biological process categories in which the strongly contributing positive and negative genes are most involved, we ran our enrichment analysis separately on the positive genes (genes with the 50% most positive loadings) and the negative genes (genes with the 50% most negative loadings). For each category, we define the category score as the mean loading of the genes in the category. The null model was constructed by permuting the rows (brain areas) of the functional association matrix while preserving spatial autocorrelation using the spherical projection and rotation procedure (spins) described in the previous subsection. We then subjected the original gene expression matrix and the permuted functional association matrix to PLS and recomputed the null gene loadings and null category scores (10 000 repetitions). Significance was assessed using a two-tailed permutation test.

Next, cell-type deconvolution was performed using cell-specific aggregate gene sets across five human adult postmortem single-cell and single-nucleus RNA sequencing studies^{43–48}, as presented previously (Supplementary Table 5 from²³). Briefly, cortical cell classes were determined based on hierarchical clustering of regional topographies across all study-specific cell types in the Allen Human Brain Atlas, resulting in seven major canonical cortical cell classes: astrocytes (Astro), endothelial (Endo), microglia (Micro), excitatory neurons (Neuro-Ex), inhibitory neurons (Neuro-In), oligodendrocytes (Oligo), and oligodendrocyte precursors (OPC) (See Figure 2 from²³).

Human Connectome Project dataset

Data from the Human Connectome Project (HCP, S1200 release)^{83,84} was used for measures of cortical thickness, T1w/T2w ratios, functional connectivity, and behavioural tests, as approved by the WU-Minn HCP Consortium. The 417 unrelated subjects (age range 22–37 years, 193 males) with available resting-state fMRI data had individual measures of cortical thickness and T1w/T2w ratios. These structural modalities were acquired on a Siemens Skyra 3T scanner, and included a T1-weighted MPRAGE sequence at an isotropic resolution of 0.7mm, and a T2-weighted SPACE also at an isotropic resolution of 0.7mm. Details on imaging protocols and procedures are available at <http://protocols.humanconnectome.org/HCP/3T/imaging-protocols.html>. Image processing includes correcting for gradient distortion caused by nonlinearities, correcting for bias field distortions, and registering the images to a standard reference space. Measures of cortical thickness are estimated as the geometric distance between the white and grey matter surfaces,

and intracortical myelin as the T1w/T2w ratio. Cortical thickness and T1w/T2w ratios for each subject was made available in the surface-based CIFTI file format and parcellated into 219 cortical regions according to the Lausanne anatomical atlas³². Only the left-hemisphere regions were retained for analysis.

A group-averaged dense functional connectivity matrix was constructed from the 1 003 subjects with all four 15-minute resting-state fMRI runs. For details on how the dense functional connectivity matrix was constructed, see <https://www.humanconnectome.org/storage/app/media/documentation/s1200/HCP1200-DenseConnectome+PTN+Appendix-July2017.pdf>. The cortical subset of the matrix was parcellated into 219 nodes according to the Lausanne anatomical atlas³². Following Margulies and colleagues, a principal functional gradient was computed by applying diffusion map embedding to the functional connectivity matrix⁵⁶, using the Dimensionality Reduction Toolbox (<https://lvdmaaten.github.io/drtoolbox/>). The procedure yielded an eigenvector map representing the differentiation of unimodal and transmodal cortical regions. Only the left hemisphere was retained for comparison with gene and term scores.

Robustness analysis using BrainMap

BrainMap is a manually created and curated data repository of results from published functional and structural neuroimaging studies^{17,59–61}. Specifically, BrainMap includes the brain coordinates that are significantly activated during thousands of different experiments. All experiments conducted on unhealthy subjects were excluded, as well as all experiments without a defined behavioural domain. This resulted in 8 703 experiments organized into 66 unique behavioural domains (Supplementary Table 2). To enable more direct comparability with results using Neurosynth, the BrainMap data were subjected to the Neurosynth meta-analytic pipeline (<https://github.com/neurosynth/neurosynth>). Note that Neurosynth terms and BrainMap behavioural domains differ considerably, making term comparison challenging (see Supplementary Table 1 versus Supplementary Table 2). This approach resulted in a region by term matrix of probabilistic measures that certain terms are published in conjunction with certain brain regions.

Robustness analysis using BrainSpan

BrainSpan is a database of gene expression in the brain across development, available at <https://www.brainspan.org/static/download.html>²². Gene expression levels were quantified in specific tissue samples from post-mortem brains ranging from eight post-conception weeks (pcw) to 40 years of age. Ages were binned

into five life stages: fetus (8pcw–37pcw), infant (4mos–1yr), child (2yrs–8yrs), adolescent (11yrs–19yrs), and adult (21yrs–40yrs)⁸⁵. For each age category, a gene expression matrix was constructed by averaging the expression of every gene across identical regions, ignoring the genes without any expression values (0.057% of the data). Genes with no estimated expression level in a particular brain region across all samples in a life stage were imputed using the median gene expression across all genes in that brain region; this interpolation occurred infrequently (0.022% of the time). Of the sixteen unique cortical brain regions with gene expression levels, four regions did not have gene expression estimates in any of the age categories besides the fetal stage. Therefore, only gene scores in the twelve consistent brain regions were tracked across life stages. For comparison with PLS results derived from AHBA, we selected the 8 607 available genes with differential stability greater than 0.1 as defined on the 34-node parcellation, and complete sample data across all brain regions for each life stage. Gene scores for the twelve regions with expression levels available for all age stages were estimated by multiplying the gene expression matrices and the PLS-derived gene weights (columns of U).

To relate estimated gene scores with term scores, we defined a region-to-region correspondence map from the 16-node parcellation to the 34-node parcellation. Term scores were averaged across sibling nodes such that a single term score was available for all 16 regions available in BrainSpan. Note that brain regions in BrainSpan are not organized by hemisphere; therefore, regional expression levels in the 16 regions are not necessarily measured from the left hemisphere only. Furthermore, due to the small sample of cortical brain regions, gene expression estimates are much less specific compared to the AHBA dataset.

Data availability

The Allen Human Brain Atlas is available at <https://human.brain-map.org/static/download>, the Neurosynth database is available at <https://neurosynth.org/>, the Human Connectome Project database is available at https://db.humanconnectome.org/data/projects/HCP_1200, and the BrainSpan database is available at <https://www.brainspan.org/static/download.html>. Processed data as used in this report are available at https://github.com/netneurolab/hansen_genescognition. BrainMap data is available upon reasonable request to BM.

Code availability

Code used to conduct the reported analyses are available at https://github.com/netneurolab/hansen_genescognition.

Acknowledgments

We thank Vincent Bazinet, Laura Suarez, Golia Shafiei, Bertha Vazquez-Rodriguez and Zhen-Qi Liu for their comments and suggestions on the manuscript. This research was undertaken thanks in part to funding from the Canada First Research Excellence Fund, awarded to McGill University for the Healthy Brains for Healthy Lives initiative. BM acknowledges support from the Natural Sciences and Engineering Research Council of Canada (NSERC Discovery Grant RGPIN #017-04265) and from the Canada Research Chairs Program. JWV was funded by the NIH grant T32MH019112. DB was supported by the Healthy Brains Healthy Lives initiative (Canada First Research Excellence fund), the CIFAR Artificial Intelligence Chairs program (Canada Institute for Advanced Research), Google (Research Award), and by NIH grant

R01AG068563A. The funders had no role in study design, data collection and analysis, decision to publish or preparation of the manuscript.

Author contributions

JYH and BM conceived the study. JYH performed the formal analysis, with contribution from RDM. RDM, JWV, JS, and DB contributed data. JYH and BM wrote the manuscript, with valuable revision by RDM, JWV, JS, and DB. BM was the project administrator.

Competing interests

The authors declare no competing interests.

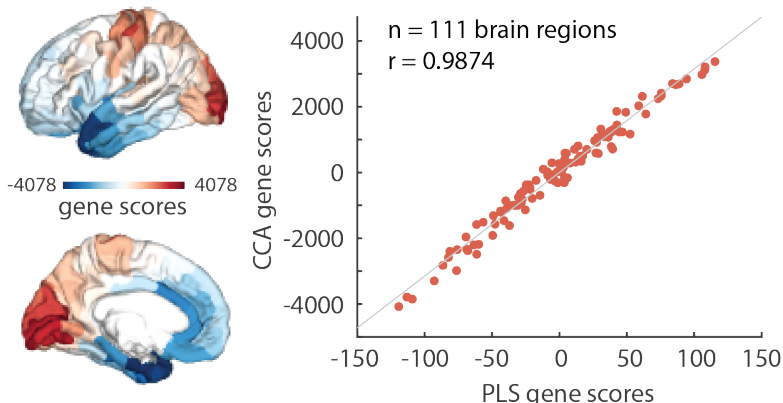
- [1] Richard F Betzel and Danielle S Bassett. Multi-scale brain networks. *Neuroimage*, 160:73–83, 2017.
- [2] Shreejoy J Tripathy, Lilah Toker, Brenna Li, Cindy-Lee Crichlow, Dmitry Tebaykin, B Ogan Mancarci, and Paul Pavlidis. Transcriptomic correlates of neuron electrophysiological diversity. *PLoS Comput Biol*, 13(10):e1005814, 2017.
- [3] Cathryn R Cadwell, Athanasia Palasantza, Xiaolong Jiang, Philipp Berens, Qiaolin Deng, Marlene Yilmaz, Jacob Reimer, Shan Shen, Matthias Bethge, Kimberley F Tolias, et al. Electrophysiological, transcriptomic and morphologic profiling of single neurons using patch-seq. *Nat Biotech*, 34(2):199–203, 2016.
- [4] Kevin FH Lee, Cary Soares, Jean-Philippe Thivierge, and Jean-Claude Béique. Correlated synaptic inputs drive dendritic calcium amplification and cooperative plasticity during clustered synapse development. *Neuron*, 89(4):784–799, 2016.
- [5] Nicolas Frémaux and Wulfram Gerstner. Neuromodulated spike-timing-dependent plasticity, and theory of three-factor learning rules. *Frontiers in neural circuits*, 9:85, 2016.
- [6] Aaron G Blankenship and Marla B Feller. Mechanisms underlying spontaneous patterned activity in developing neural circuits. *Nat Rev Neurosci*, 11(1):18–29, 2010.
- [7] Gwendolyn G Calhoun and Kay M Tye. Resolving the neural circuits of anxiety. *Nature neuroscience*, 18(10):1394–1404, 2015.
- [8] Laura E Suárez, Ross D Markello, Richard F Betzel, and Bratislav Misic. Linking structure and function in macroscale brain networks. *Trends Cogn Sci*, 2020.
- [9] BT Yeo, Fenna M Krienen, Jorge Sepulcre, Mert R Sabuncu, Danial Lashkari, Marisa Hollinshead, Joshua R Roffman, Jordan W Smoller, Lilla Zöllei, Jonathan R Polimeni, et al. The organization of the human cerebral cortex estimated by intrinsic functional connectivity. *J Neurophysiol*, 106(3):1125–1165, 2011.
- [10] Jessica S Damoiseaux, SARB Rombouts, Frederik Barkhof, Philip Scheltens, Cornelis J Stam, Stephen M Smith, and Christian F Beckmann. Consistent resting-state networks across healthy subjects. *Proc Natl Acad Sci USA*, 103(37):13848–13853, 2006.
- [11] Jonas Richiardi, Andre Altmann, Anna-Clare Milazzo, Catie Chang, M Mallar Chakravarty, Tobias Banaschewski, Gareth J Barker, Arun LW Bokde, Uli Bromberg, Christian Büchel, et al. Correlated gene expression supports synchronous activity in brain networks. *Science*, 348(6240):1241–1244, 2015.
- [12] Ben D Fulcher and Alex Fornito. A transcriptional signature of hub connectivity in the mouse connectome. *Proc Natl Acad Sci USA*, 113(5):1435–1440, 2016.
- [13] Ben D Fulcher, John D Murray, Valerio Zerbi, and Xiao-Jing Wang. Multimodal gradients across mouse cortex. *Proc Natl Acad Sci USA*, 116(10):4689–4695, 2019.
- [14] Richard F Betzel, John D Medaglia, Ari E Kahn, Jonathan Soffer, Daniel R Schonhaut, and Danielle S Bassett. Structural, geometric and genetic factors predict interregional brain connectivity patterns probed by electrocorticography. *Nat Biomed Eng*, 3(11):902–916, 2019.
- [15] PE Vértes, T Rittman, KJ Whitaker, R Romero-Garcia, F Váša, M Kitzbichler, P Fonagy, RJ Dolan, PB Jones, IM Goodyer, et al. Gene transcription profiles associated with intra-modular and inter-modular hubs in human fmri networks. *Philos Trans R Soc Lond B Biol Sci*, 371:735–769, 2016.
- [16] Tal Yarkoni, Russell A Poldrack, Thomas E Nichols, David C Van Essen, and Tor D Wager. Large-scale automated synthesis of human functional neuroimaging data. *Nat Meth*, 8(8):665, 2011.
- [17] Peter T Fox and Jack L Lancaster. Mapping context and content: the brainmap model. *Nature Reviews Neuroscience*, 3(4):319–321, 2002.
- [18] Krzysztof J Gorgolewski, Gael Varoquaux, Gabriel Rivera, Yannick Schwarz, Satrajit S Ghosh, Camille Maumet, Vanessa V Sochat, Thomas E Nichols, Russell A Poldrack, Jean-Baptiste Poline, et al. Neurovault.org: a web-based repository for collecting and sharing unthresholded statistical maps of the human brain. *Front Neuroinform*, 9:8, 2015.
- [19] Jérôme Dockès, Russell A Poldrack, Romain Primet, Hande Gözükhan, Tal Yarkoni, Fabian Suchanek, Bertrand Thirion, and Gaël Varoquaux. Neuroquery, comprehen-

- sive meta-analysis of human brain mapping. *eLife*, 9:e53385, 2020.
- [20] Michael J Hawrylycz, Ed S Lein, Angela L Guillozet-Bongaarts, Elaine H Shen, Lydia Ng, Jeremy A Miller, Louie N Van De Lagemaat, Kimberly A Smith, Amanda Ebbert, Zackery L Riley, et al. An anatomically comprehensive atlas of the adult human brain transcriptome. *Nature*, 489(7416):391, 2012.
- [21] Michael Hawrylycz, Jeremy A Miller, Vilas Menon, David Feng, Tim Dolbeare, Angela L Guillozet-Bongaarts, Anil G Jegga, Bruce J Aronow, Chang-Kyu Lee, Amy Bernard, et al. Canonical genetic signatures of the adult human brain. *Nat Neurosci*, 18(12):1832, 2015.
- [22] Jeremy A Miller, Song-Lin Ding, Susan M Sunkin, Kimberly A Smith, Lydia Ng, Aaron Szafer, Amanda Ebbert, Zackery L Riley, Joshua J Royall, Kaylynn Aiona, et al. Transcriptional landscape of the prenatal human brain. *Nature*, 508(7495):199–206, 2014.
- [23] Jakob Seidlitz, Ajay Nadig, Siyuan Liu, Richard AI Bethlehem, Petra E Vértes, Sarah E Morgan, František Váša, Rafael Romero-Garcia, François M Lalonde, Liv S Clasen, et al. Transcriptomic and cellular decoding of regional brain vulnerability to neurodevelopmental disorders. *Nature Communications*, .(.).., 2020.
- [24] Kirstie J Whitaker, Petra E Vértes, Rafael Romero-Garcia, František Váša, Michael Moutoussis, Gita Prabhu, Niklaus Weiskopf, Martina F Callaghan, Konrad Wagstyl, Timothy Rittman, et al. Adolescence is associated with genomically patterned consolidation of the hubs of the human brain connectome. *Proceedings of the National Academy of Sciences*, 113(32):9105–9110, 2016.
- [25] František Váša, Rafael Romero-Garcia, Manfred G Kitzbichler, Jakob Seidlitz, Kirstie J Whitaker, Matilde M Vaghi, Prantik Kundu, Ameera X Patel, Peter Fonagy, Raymond J Dolan, et al. Conservative and disruptive modes of adolescent change in human brain functional connectivity. *Proc Natl Acad Sci USA*, 117(6):3248–3253, 2020.
- [26] Joshua B Burt, Murat Demirtaş, William J Eckner, Natasha M Navejar, Jie Lisa Ji, William J Martin, Alberto Bernacchia, Alan Anticevic, and John D Murray. Hierarchy of transcriptomic specialization across human cortex captured by structural neuroimaging topography. *Nature neuroscience*, 21(9):1251–1259, 2018.
- [27] Aurina Arnatkevičiūtė, Ben D Fulcher, and Alex Fornito. A practical guide to linking brain-wide gene expression and neuroimaging data. *Neuroimage*, 189:353–367, 2019.
- [28] Andrew S Fox, Luke J Chang, Krzysztof J Gorgolewski, and Tal Yarkoni. Bridging psychology and genetics using large-scale spatial analysis of neuroimaging and neurogenetic data. *bioRxiv*, page 012310, 2014.
- [29] Aaron F Alexander-Bloch, Haochang Shou, Siyuan Liu, Theodore D Satterthwaite, David C Glahn, Russell T Shinohara, Simon N Vandekar, and Armin Raznahan. On testing for spatial correspondence between maps of human brain structure and function. *NeuroImage*, 178:540–551, 2018.
- [30] Russell A Poldrack, Aniket Kittur, Donald Kalar, Eric Miller, Christian Seppa, Yolanda Gil, D Stott Parker, Fred W Sabb, and Robert M Bilder. The cognitive atlas: toward a knowledge foundation for cognitive neuroscience. *Frontiers Neuroinform*, 5:17, 2011.
- [31] Rahul S Desikan, Florent Ségonne, Bruce Fischl, Brian T Quinn, Bradford C Dickerson, Deborah Blacker, Randy L Buckner, Anders M Dale, R Paul Maguire, Bradley T Hyman, et al. An automated labeling system for subdividing the human cerebral cortex on mri scans into gyral based regions of interest. *NeuroImage*, 31(3):968–980, 2006.
- [32] Leila Cammoun, Xavier Gigandet, Djalel Meskaldji, Jean Philippe Thiran, Olaf Sporns, Kim Q Do, Philippe Maeder, Reto Meuli, and Patric Hagmann. Mapping the human connectome at multiple scales with diffusion spectrum mri. *J Neurosci Meth*, 203(2):386–397, 2012.
- [33] AR McIntosh, FL Bookstein, James V Haxby, and CL Grady. Spatial pattern analysis of functional brain images using partial least squares. *NeuroImage*, 3(3):143–157, 1996.
- [34] Anjali Krishnan, Lynne J Williams, Anthony Randal McIntosh, and Hervé Abdi. Partial least squares (pls) methods for neuroimaging: a tutorial and review. *NeuroImage*, 56(2):455–475, 2011.
- [35] Anthony R McIntosh and Bratislav Mišić. Multivariate statistical analyses for neuroimaging data. *Annu Rev Psychol*, 64:499–525, 2013.
- [36] Bertha Vázquez-Rodríguez, Laura E Suárez, Ross D Markello, Golia Shafei, Casey Paquola, Patric Hagmann, Martijn P Van Den Heuvel, Boris C Bernhardt, R Nathan Spreng, and Bratislav Misic. Gradients of structure-function tethering across neocortex. *Proceedings of the National Academy of Sciences*, 116(42):21219–21227, 2019.
- [37] Ross Markello and Bratislav Misic. Comparing spatially-constrained null models for parcellated brain maps. *BioRxiv*, 2020.
- [38] Joshua B Burt, Markus Helmer, Maxwell Shinn, Alan Anticevic, and John D Murray. Generative modeling of brain maps with spatial autocorrelation. *NeuroImage*, 2020.
- [39] Ben D Fulcher, Aurina Arnatkevičiūtė, and Alex Fornito. Overcoming bias in gene-set enrichment analyses of brain-wide transcriptomic data. *bioRxiv*, 2020.
- [40] Constantin Freiherr von Economo and Georg N Koskinas. *Die cytoarchitektonik der hirnrinde des erwachsenen menschen*. J. Springer, 1925.
- [41] M-MARSEL Mesulam. Behavioral neuroanatomy. *Principles of behavioral and cognitive neurology*, 2:1–120, 2000.
- [42] Casey Paquola, Reinder Vos De Wael, Konrad Wagstyl, Richard AI Bethlehem, Seok-Jun Hong, Jakob Seidlitz, Edward T Bullmore, Alan C Evans, Bratislav Misic, Daniel S Margulies, et al. Microstructural and functional gradients are increasingly dissociated in transmodal cortices. *PLoS biology*, 17(5):e3000284, 2019.
- [43] Ye Zhang, Steven A Sloan, Laura E Clarke, Christine Caneda, Colton A Plaza, Paul D Blumenthal, Hannes Vogel, Gary K Steinberg, Michael SB Edwards, Gordon Li, et al. Purification and characterization of progenitor and mature human astrocytes reveals transcriptional and functional differences with mouse. *Neuron*, 89(1):37–53, 2016.
- [44] Blue B Lake, Song Chen, Brandon C Sos, Jean Fan, Gwendolyn E Kaeser, Yun C Yung, Thu E Duong, Derek Gao, Jerold Chun, Peter V Kharchenko, et al. Integrative single-cell analysis of transcriptional and epigenetic states in the human adult brain. *Nature biotechnology*, 36(1):70–80, 2018.
- [45] Naomi Habib, Inbal Avraham-Davidi, Anindita Basu, Tyler Burks, Karthik Shekhar, Matan Hofree, Sourav R Choudhury, François Aguet, Ellen Gelfand, Kristin Ardlie, et al. Massively parallel single-nucleus rna-seq with dronc-seq. *Nature methods*, 14(10):955–958, 2017.

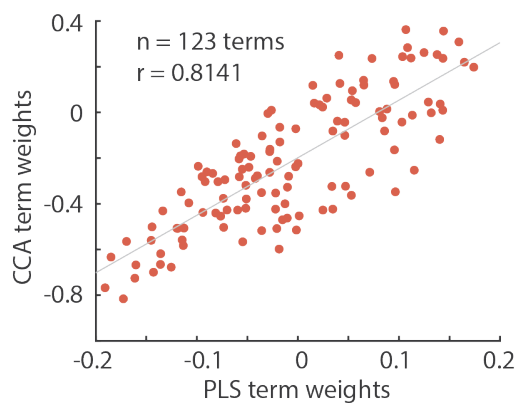
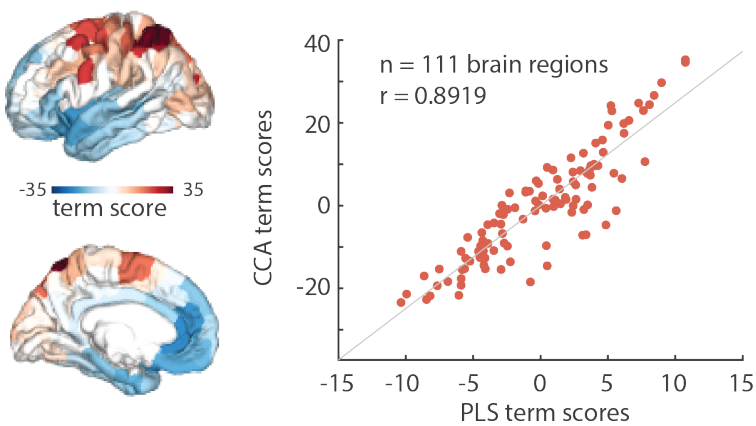
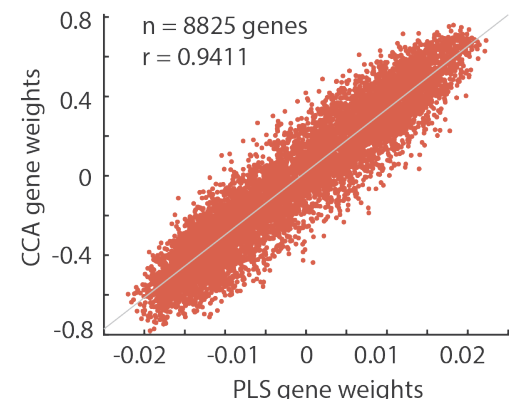
- [46] Spyros Darmanis, Steven A Sloan, Ye Zhang, Martin Enge, Christine Caneda, Lawrence M Shuer, Melanie G Hayden Gephart, Ben A Barres, and Stephen R Quake. A survey of human brain transcriptome diversity at the single cell level. *Proceedings of the National Academy of Sciences*, 112(23):7285–7290, 2015.
- [47] Mingfeng Li, Gabriel Santpere, Yuka Imamura Kawasawa, Oleg V Evgrafov, Forrest O Gulden, Sirisha Pochareddy, Susan M Sunkin, Zhen Li, Yurae Shin, Ying Zhu, et al. Integrative functional genomic analysis of human brain development and neuropsychiatric risks. *Science*, 362(6420), 2018.
- [48] Andrew T McKenzie, Minghui Wang, Mads E Hauberg, John F Fullard, Alexey Kozlenkov, Alexandra Keenan, Yasmin L Hurd, Stella Dracheva, Patrizia Casaccia, Panos Roussos, et al. Brain cell type specific gene expression and co-expression network architectures. *Scientific reports*, 8(1):1–19, 2018.
- [49] Julia M Huntenburg, Pierre-Louis Bazin, and Daniel S Margulies. Large-scale gradients in human cortical organization. *Trends Cogn Sci*, 22(1):21–31, 2018.
- [50] Xiao-Jing Wang. Macroscopic gradients of synaptic excitation and inhibition in the neocortex. *Nat Rev Neurosci*, pages 1–10, 2020.
- [51] Matthew F Glasser and David C Van Essen. Mapping human cortical areas in vivo based on myelin content as revealed by t1-and t2-weighted mri. *J Neurosci*, 31(32):11597–11616, 2011.
- [52] Konrad Wagstyl, Lisa Ronan, Ian M Goodyer, and Paul C Fletcher. Cortical thickness gradients in structural hierarchies. *NeuroImage*, 111:241–250, 2015.
- [53] Julia M Huntenburg, Pierre-Louis Bazin, Alexandros Goulas, Christine L Tardif, Arno Villringer, and Daniel S Margulies. A systematic relationship between functional connectivity and intracortical myelin in the human cerebral cortex. *Cerebral Cortex*, 27(2):981–997, 2017.
- [54] EG Jones and TPS Powell. An anatomical study of converging sensory pathways within the cerebral cortex of the monkey. *Brain*, 93(4):793–820, 1970.
- [55] M-Marsel Mesulam. From sensation to cognition. *Brain*, 121(6):1013–1052, 1998.
- [56] Daniel S Margulies, Satrajit S Ghosh, Alexandros Goulas, Marcel Falkiewicz, Julia M Huntenburg, Georg Langs, Gleb Bezgin, Simon B Eickhoff, F Xavier Castellanos, Michael Petrides, et al. Situating the default-mode network along a principal gradient of macroscale cortical organization. *Proc Natl Acad Sci USA*, 113(44):12574–12579, 2016.
- [57] Ronald R Coifman, Stephane Lafon, Ann B Lee, Mauro Maggioni, Boaz Nadler, Frederick Warner, and Steven W Zucker. Geometric diffusions as a tool for harmonic analysis and structure definition of data: Diffusion maps. *Proc Natl Acad Sci USA*, 102(21):7426–7431, 2005.
- [58] Laurens Van Der Maaten, Eric Postma, and Jaap Van den Herik. Dimensionality reduction: a comparative. *J Mach Learn Res*, 10:66–71, 2009.
- [59] Peter T Fox, Angela R Laird, Sarabeth P Fox, P Mickle Fox, Angela M Uecker, Michelle Crank, Sandra F Koenig, and Jack L Lancaster. Brainmap taxonomy of experimental design: description and evaluation. *Human brain mapping*, 25(1):185–198, 2005.
- [60] Thomas J Vanasse, P Mickle Fox, Daniel S Barron, Michaela Robertson, Simon B Eickhoff, Jack L Lancaster, and Peter T Fox. Brainmap vbm: An environment for structural meta-analysis. *Human brain mapping*, 39(8):3308–3325, 2018.
- [61] Angela R Laird, Jack J Lancaster, and Peter T Fox. Brainmap. *Neuroinformatics*, 3(1):65–77, 2005.
- [62] Aaron F Alexander-Bloch, Armin Raznahan, Simon N Vandekar, Jakob Seidlitz, Zhixin Lu, Samuel R Matthias, Emma Knowles, Josephine Mollon, Amanda Rodrigue, Joanne E Curran, et al. Imaging local genetic influences on cortical folding. *Proceedings of the National Academy of Sciences*, 117(13):7430–7436, 2020.
- [63] Marie Forest, Yasser Iturria-Medina, Jennifer S Goldman, Claudia L Kleinman, Amanda Lovato, Kathleen Oros Klein, Alan Evans, Antonio Ciampi, Aurélie Labbe, and Celia MT Greenwood. Gene networks show associations with seed region connectivity. *Human brain mapping*, 38(6):3126–3140, 2017.
- [64] Fenna M Krienen, BT Thomas Yeo, Tian Ge, Randy L Buckner, and Chet C Sherwood. Transcriptional profiles of supragranular-enriched genes associate with corticocortical network architecture in the human brain. *Proceedings of the National Academy of Sciences*, 113(4):E469–E478, 2016.
- [65] Randy L Buckner and Fenna M Krienen. The evolution of distributed association networks in the human brain. *Trends in cognitive sciences*, 17(12):648–665, 2013.
- [66] Sophia Mueller, Danhong Wang, Michael D Fox, BT Thomas Yeo, Jorge Sepulcre, Mert R Sabuncu, Rebecca Shafee, Jie Lu, and Hesheng Liu. Individual variability in functional connectivity architecture of the human brain. *Neuron*, 77(3):586–595, 2013.
- [67] Younghun Jo, Joshua Faskowitz, Farnaz Zamani Esfahlani, Olaf Sporns, and Richard F Betzel. Subject identification using edge-centric functional connectivity. *bioRxiv*, 2020.
- [68] Jacob W Vogel, Renaud La Joie, Michel J Grothe, Alexandre Diaz-Papkovich, Andrew Doyle, Etienne Vachon-Presseau, Claude Lepage, Reinder Vos de Wael, Rhalena A Thomas, Yasser Iturria-Medina, et al. A molecular gradient along the longitudinal axis of the human hippocampus informs large-scale behavioral systems. *Nat Commun*, 11(1):1–17, 2020.
- [69] Bratislav Mišić and Olaf Sporns. From regions to connections and networks: new bridges between brain and behavior. *Curr Opin Neurobiol*, 40:1–7, 2016.
- [70] Matthias Kirschner, Golia Shafiei, Ross D Markello, Carolina Makowski, Alexandra Talpalaru, Benazir Hodzic-Santor, Gabriel A Devenyi, Casey Paquola, Boris C Bernhardt, Martin Lepage, et al. Latent clinical-anatomical dimensions of schizophrenia. *Schizophrenia Bulletin*, 46(6):1426–1438, 2020.
- [71] Sandra Amor, Fabiola Puentes, David Baker, and Paul Van Der Valk. Inflammation in neurodegenerative diseases. *Immunology*, 129(2):154–169, 2010.
- [72] Golia Shafiei, Ross D Markello, Carolina Makowski, Alexandra Talpalaru, Matthias Kirschner, Gabriel A Devenyi, Elisa Guma, Patric Hagmann, Neil R Cashman, Martin Lepage, et al. Spatial patterning of tissue volume loss in schizophrenia reflects brain network architecture. *Biological psychiatry*, 87(8):727–735, 2020.
- [73] George Bush, Phan Luu, and Michael I Posner. Cognitive and emotional influences in anterior cingulate cortex. *Trends in cognitive sciences*, 4(6):215–222, 2000.
- [74] Madeleine Goodkind, Simon B Eickhoff, Desmond J Oathes, Ying Jiang, Andrew Chang, Laura B Jones-

- Hagata, Brissa N Ortega, Yevgeniya V Zaiko, Erika L Roach, Mayuresh S Korgaonkar, et al. Identification of a common neurobiological substrate for mental illness. *JAMA psychiatry*, 72(4):305–315, 2015.
- [75] Alice Patania, Pierluigi Selvaggi, Mattia Veronese, Ottavia Dipasquale, Paul Expert, and Giovanni Petri. Topological gene expression networks recapitulate brain anatomy and function. *Network Neuroscience*, 3(3):744–762, 2019.
- [76] Jeremy A Miller, Vilas Menon, Jeff Goldy, Ajamete Kaykas, Chang-Kyu Lee, Kimberly A Smith, Elaine H Shen, John W Phillips, Ed S Lein, and Mike J Hawrylycz. Improving reliability and absolute quantification of human brain microarray data by filtering and scaling probes using rna-seq. *BMC genomics*, 15(1):1–14, 2014.
- [77] Carl Eckart and Gale Young. The approximation of one matrix by another of lower rank. *Psychometrika*, 1(3): 211–218, 1936.
- [78] Natasa Kovacevic, Hervé Abdi, Derek Beaton, and Anthony R McIntosh. Revisiting pls resampling: comparing significance versus reliability across range of simulations. In *New perspectives in partial least squares and related methods*, pages 159–170. Springer, 2013.
- [79] Markus Helmer, Shaun D Warrington, Ali-Reza Mohammadi-Nejad, Jie Lisa Ji, Amber Howell, Benjamin Rosand, Alan Anticevic, Stamatis N Sotiropoulos, and John D Murray. On stability of canonical correlation analysis and partial least squares with application to brain-behavior associations. *bioRxiv*, 2020.
- [80] Harold Hotelling. Canonical correlation analysis (cca). *Journal of Educational Psychology*, page 10, 1935.
- [81] Anthony Randal McIntosh and Nancy J Lobaugh. Partial least squares analysis of neuroimaging data: applications and advances. *Neuroimage*, 23:S250–S263, 2004.
- [82] Aravind Subramanian, Pablo Tamayo, Vamsi K Mootha, Sayan Mukherjee, Benjamin L Ebert, Michael A Gillette, Amanda Paulovich, Scott L Pomeroy, Todd R Golub, Eric S Lander, et al. Gene set enrichment analysis: a knowledge-based approach for interpreting genome-wide expression profiles. *Proceedings of the National Academy of Sciences*, 102(43):15545–15550, 2005.
- [83] David C Van Essen, Stephen M Smith, Deanna M Barch, Timothy EJ Behrens, Essa Yacoub, Kamil Ugurbil, Wu-Minn HCP Consortium, et al. The wu-minn human connectome project: an overview. *Neuroimage*, 80:62–79, 2013.
- [84] Matthew F Glasser, Stamatis N Sotiropoulos, J Anthony Wilson, Timothy S Coalson, Bruce Fischl, Jesper L Andersson, Junqian Xu, Saad Jbabdi, Matthew Webster, Jonathan R Polimeni, et al. The minimal preprocessing pipelines for the human connectome project. *Neuroimage*, 80:105–124, 2013.
- [85] Donna M Werling, Sirisha Pochareddy, Jinmyung Choi, Joon-Yong An, Brooke Sheppard, Minshi Peng, Zhen Li, Claudia Dastmalchi, Gabriel Santpere, Andre MM Sousa, et al. Whole-genome and rna sequencing reveal variation and transcriptomic coordination in the developing human prefrontal cortex. *Cell Reports*, 31(1):107489, 2020.

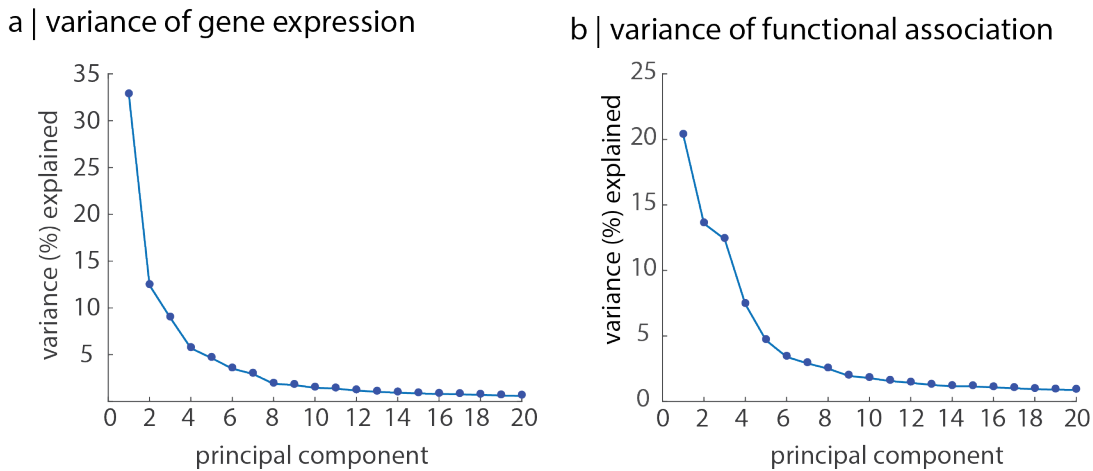
a | PLS versus CCA gene and term scores



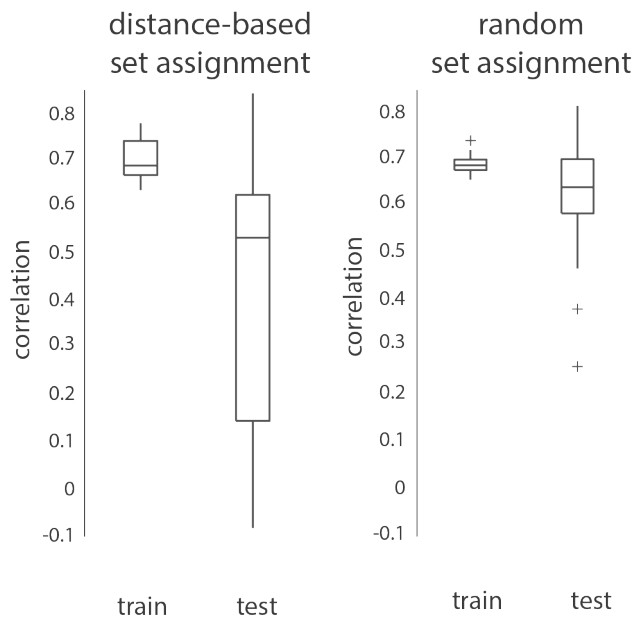
b | PLS versus CCA gene and term weights



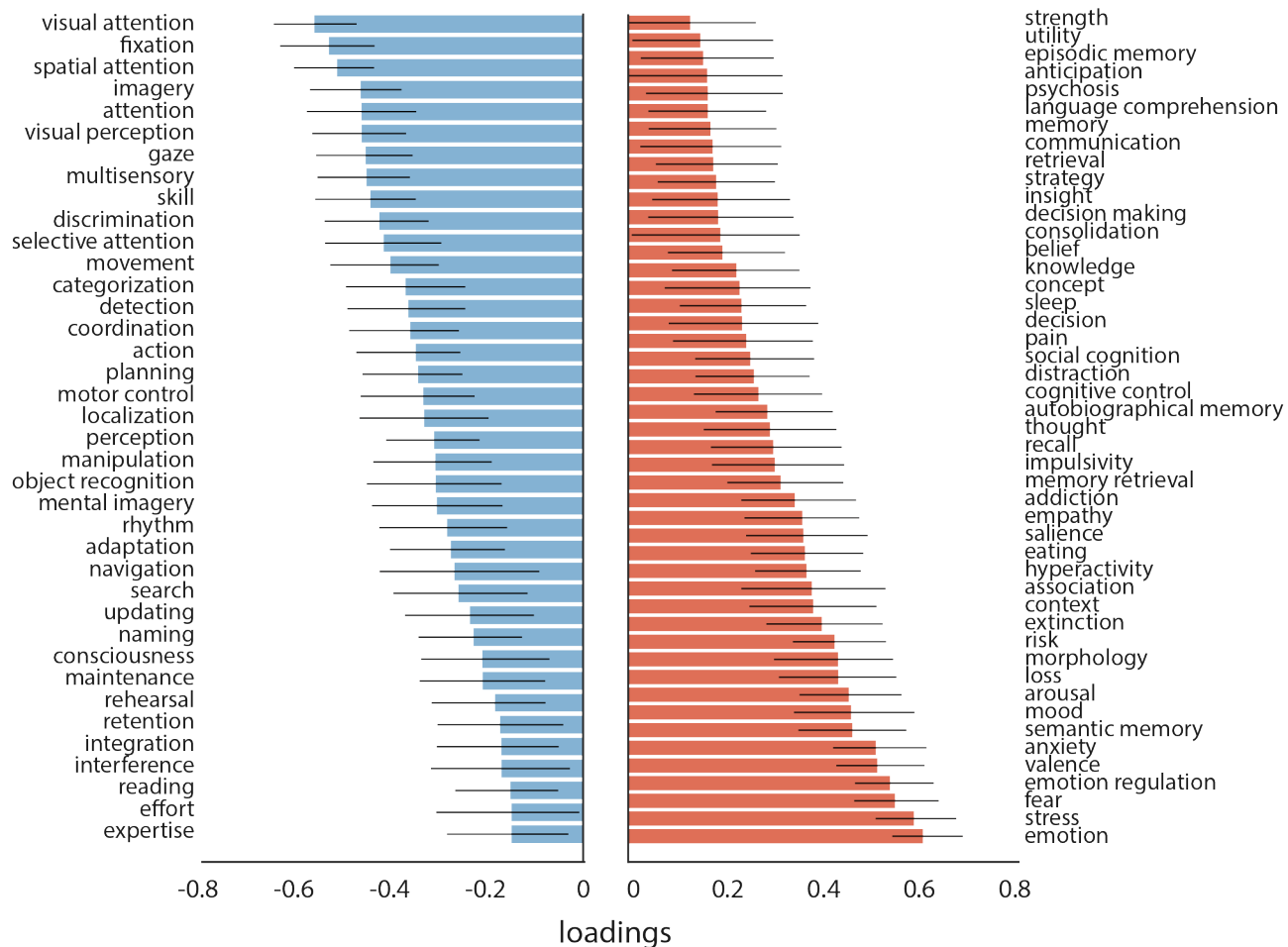
Supplementary Figure 1. Canonical correlation analysis yields similar results | Analysis were repeated using canonical correlation analysis (CCA). (a) The CCA-derived gene (top) and term (bottom) score patterns are highly similar to the PLS-derived gene and term score patterns ($n = 111$ brain regions). (b) Likewise, the CCA-derived gene (top) and term (bottom) weights are highly similar to the PLS-derived gene and term weights ($n = 8825$ genes and $n = 123$ terms).



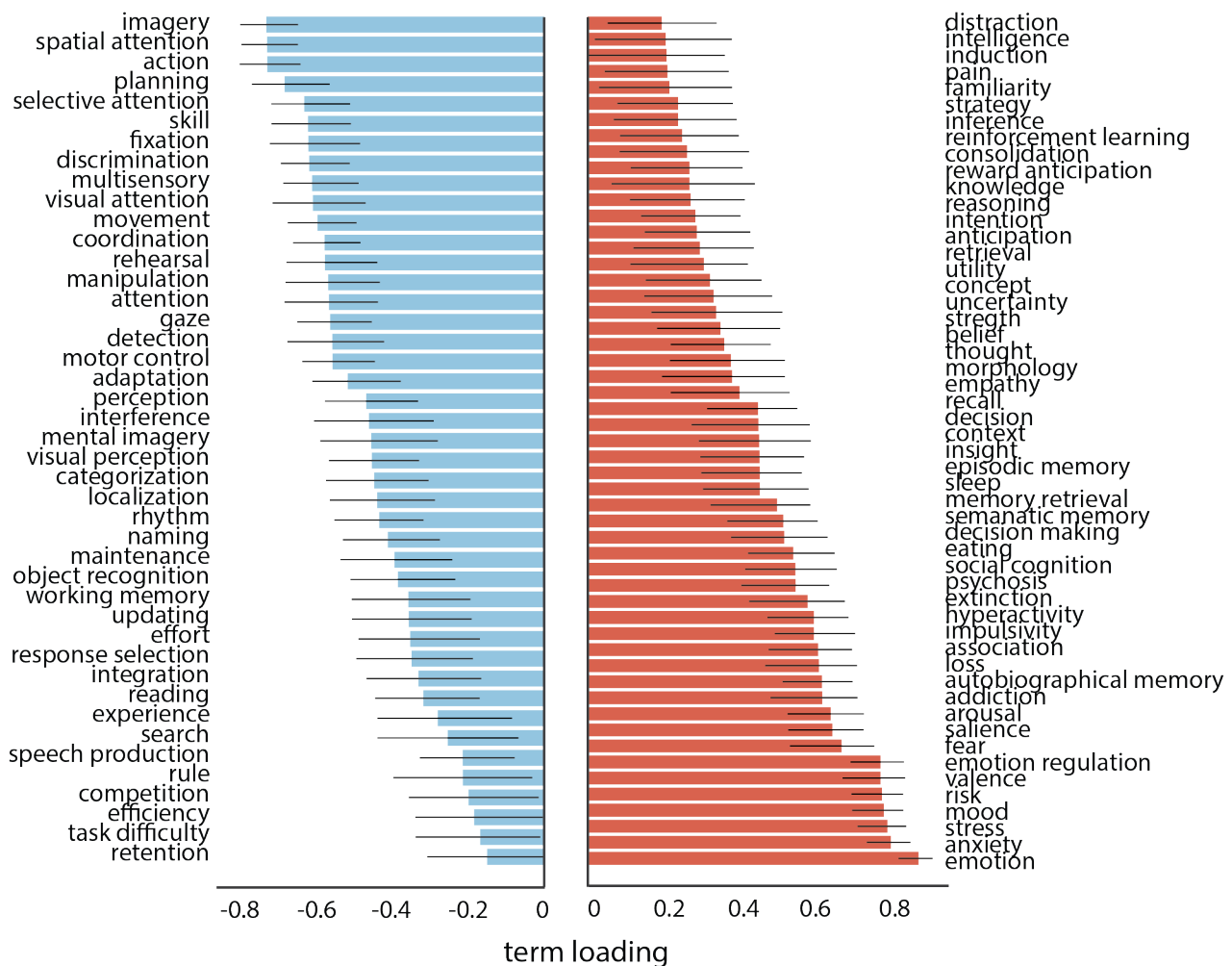
Supplementary Figure 2. Variance explained of individual datasets | Principal component analysis was applied to normalized gene expression and term functional association matrices. (a) The first principal component of gene expression explains 32.8% of the variance in the original data. (b) The first principal component of functional associations explains 20.3% of the variance in the original data.



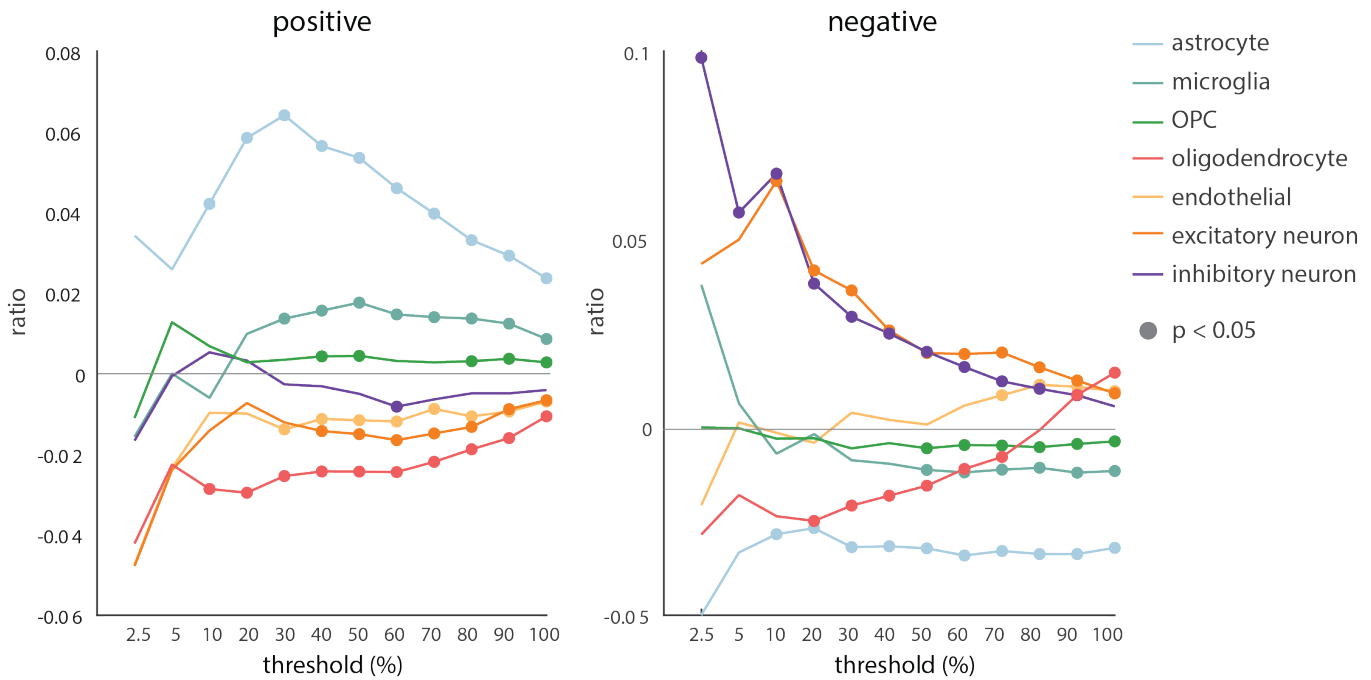
Supplementary Figure 3. Cross-validation using distance-based set assignment results in more conservative score correlations | Left: In distance-based set assignment, the 75% of nodes closest to a randomly chosen source node are assigned to the training set, and the remaining 25% of nodes are assigned to the testing set. Right: In random set assignment, training and test sets are assigned randomly. Due to spatial autocorrelation, random assignment yields inflated out-of-sample performance estimates. Only distance-based assignment was used in the manuscript. Random set assignment is shown only for comparison. Correlations are computed as Pearson's linear correlation coefficient, boxplots represent the 1st, 2nd (median) and 3rd quartiles, whiskers represent the non-outlier end-points of the distribution, and crosses represent outliers; $n = 100$ repetitions.



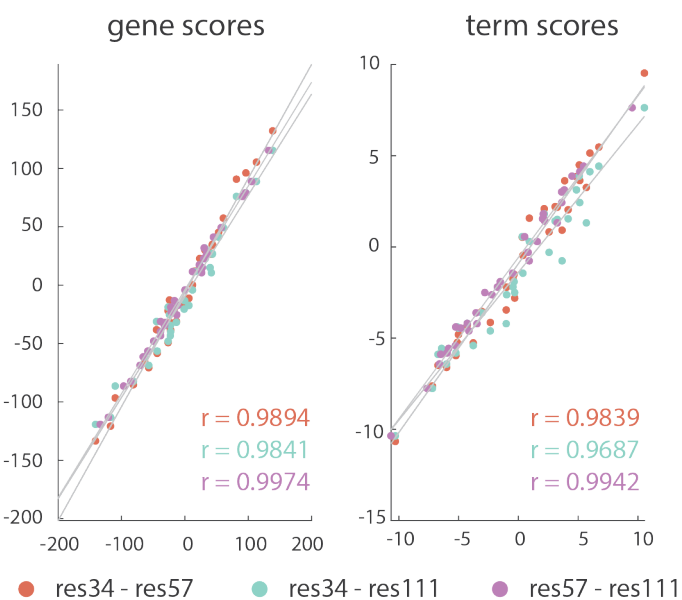
Supplementary Figure 4. **Neurosynth term loadings** | The loading for each term is calculated as the Pearson's correlation between functional associations across brain regions and PLS-derived gene scores. Error bars indicate bootstrap-estimated 95% confidence intervals (10 000 bootstrap samples). All terms with a confidence interval that changes sign are excluded.



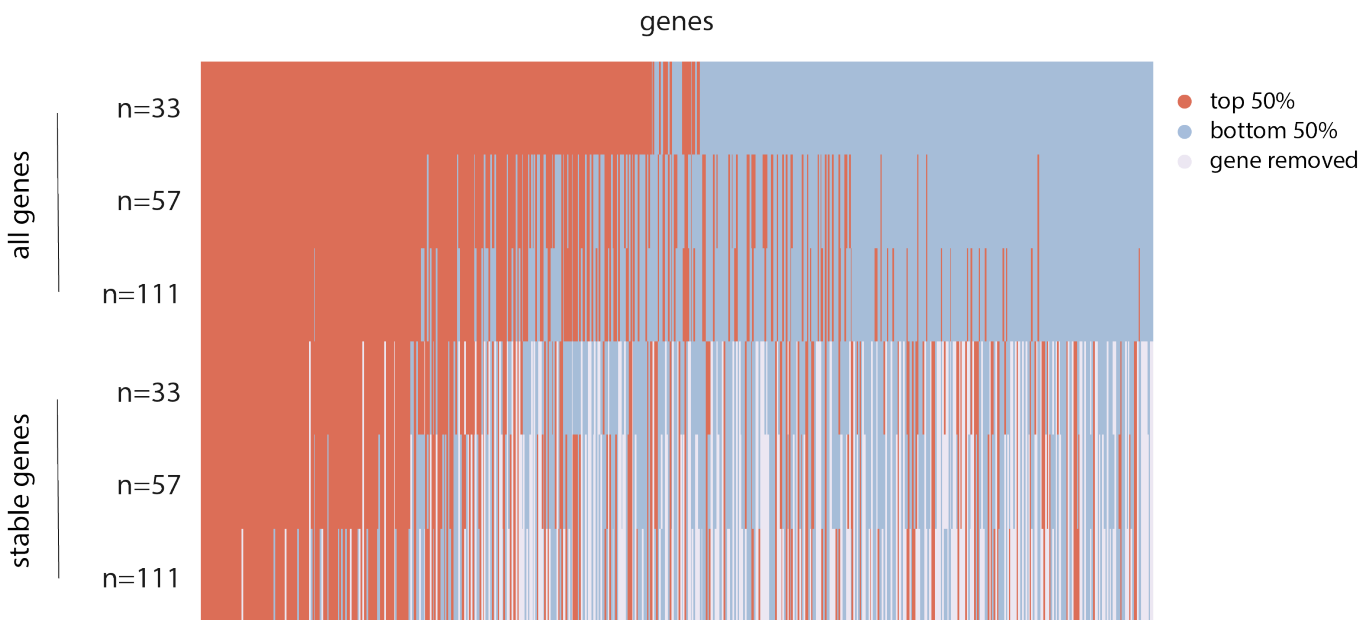
Supplementary Figure 5. **Alternative Neurosynth term loadings** | The loading for each term can be calculated as the Pearson's correlation between functional associations across brain regions and the PLS-derived term score pattern. Error bars indicate bootstrap-estimated 95% confidence intervals (10 000 bootstrap samples). All terms with a confidence interval that changes sign are excluded.



Supplementary Figure 6. Specific cell-type expression is consistent across gene sets | Positive and negative gene sets were constructed using the largest positive/negative loadings, ranging from the top 2.5% genes to all genes. Each curve represents the difference between the ratio of genes in each gene set preferentially expressed in a cell-type and the mean null ratio, computed from random gene sets (10 000 repetitions). Curves above zero indicate overexpression and curves below zero indicate underexpression. Circles demonstrate significance.



Supplementary Figure 7. Gene and term scores are consistent across parcellation resolutions | PLS was performed on gene expression and functional association matrices at three progressively finer parcellation resolutions ($n = 34$, $n = 57$, and $n = 111$ left hemisphere cortical regions;³²). The resulting gene and term scores at each resolution were then correlated with the gene and term scores from other resolutions.

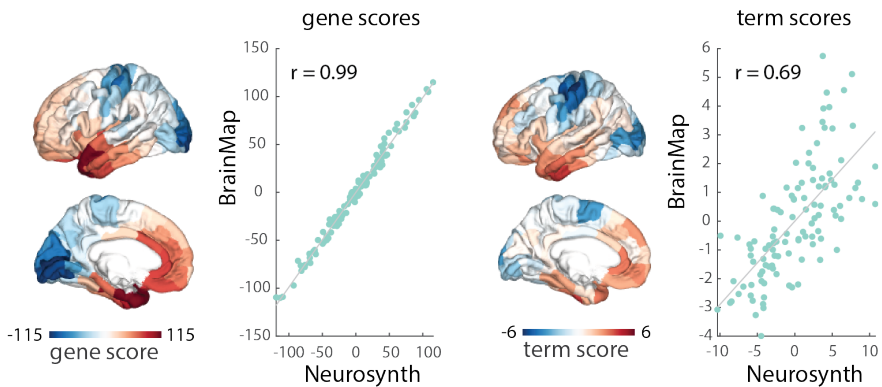


Supplementary Figure 8. Reliable gene sets are consistent across parcellation resolutions and gene set assignment | The reliability of each gene, as defined by its loading, was recomputed for six different gene expression matrices (3 parcellation resolutions \times 2 gene set assignment strategies). Tuning the parcellation of brain regions ($n = 34$, $n = 57$, and $n = 111$ left hemisphere cortical regions) and the set of genes (all genes or differentially stable genes) used in the gene expression matrix reveals reliable gene sets are consistent across different methodological choices when constructing the gene expression matrix. Reliable genes are coloured red (top 50% of positive/negative loadings), unreliable genes are blue (bottom 50% of positive/negative loadings), and genes removed from the analysis because their differential stability is less than 0.1 are white.

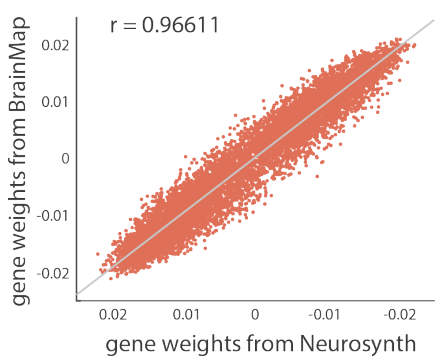
action	eating	insight	naming	semantic memory
adaptation	efficiency	integration	navigation	sentence comprehension
addiction	effort	intelligence	object recognition	skill
anticipation	emotion	intention	pain	sleep
anxiety	emotion regulation	interference	perception	social cognition
arousal	empathy	judgment	planning	spatial attention
association	encoding	knowledge	priming	speech perception
attention	episodic memory	language	psychosis	speech production
autobiographical memory	expectancy	language comprehension	reading	strategy
balance	expertise	learning	reasoning	strength
belief	extinction	listening	recall	stress
categorization	face recognition	localization	recognition	sustained attention
cognitive control	facial expression	loss	rehearsal	task difficulty
communication	familiarity	maintenance	reinforcement learning	thought
competition	fear	manipulation	response inhibition	uncertainty
concept	fixation	meaning	response selection	updating
consciousness	focus	memory	retention	utility
consolidation	gaze	memory retrieval	retrieval	valence
context	goal	mental imagery	reward anticipation	verbal fluency
coordination	hyperactivity	monitoring	rhythm	visual attention
decision	imagery	mood	risk	visual perception
decision making	impulsivity	morphology	rule	word recognition
detection	induction	motor control	salience	working memory
discrimination	inference	movement	search	
distraction	inhibition	multisensory	selective attention	

Supplementary Table 1. Neurosynth terms | Terms that overlapped between the Neurosynth database¹⁶ and the Cognitive Atlas³⁰ were included in analyses.

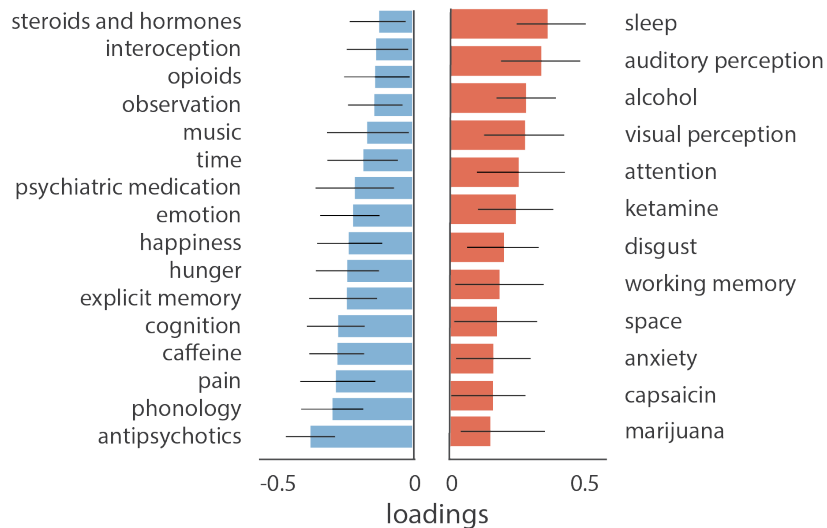
a | gene and term scores



b | correlation of gene weights

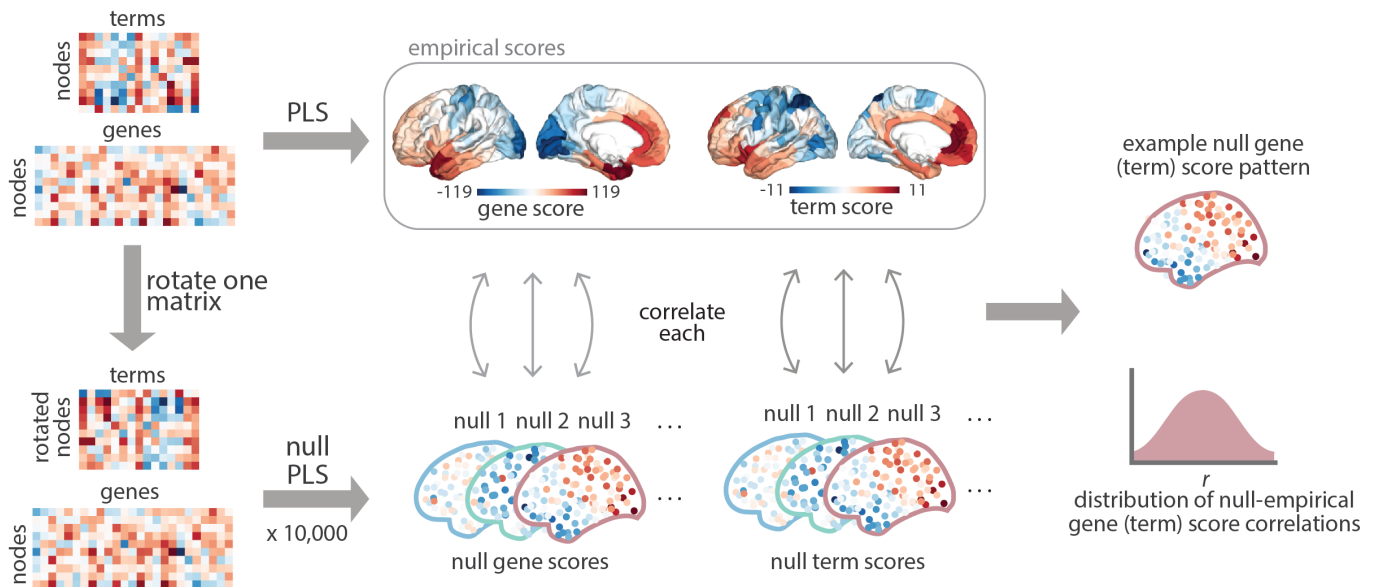


c | term loadings

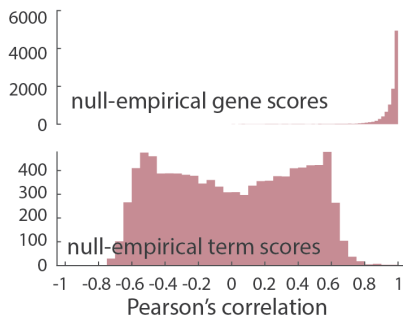
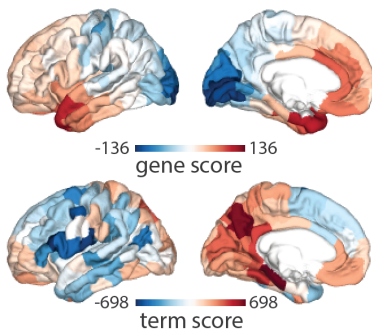


Supplementary Figure 9. Replication using BrainMap | Gene expression was related to a functional association matrix derived using the manually-curated BrainMap^{17,59}. (a) PLS-derived gene and term scores are correlated between Neurosynth- and BrainMap-derived functional association matrices ($n = 111$ brain regions). (b) PLS-estimated gene weights for the first latent variable from the Neurosynth- and BrainMap-derived functional association matrix are correlated (Pearson's r ; $n = 8825$ genes). (c) Reliable terms with positive loadings (red) and negative loadings (blue). Error bars indicate bootstrap-estimated 95% confidence intervals (10 000 bootstrap samples).

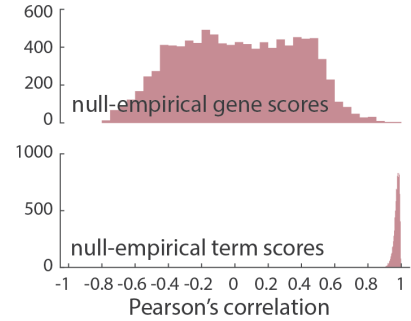
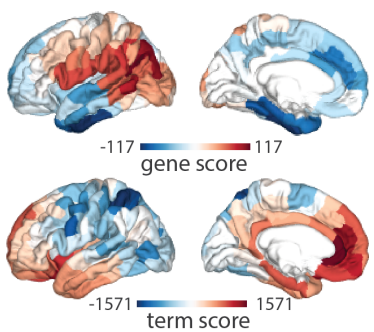
a | empirical and null PLS analysis



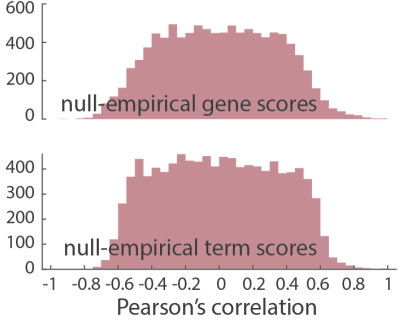
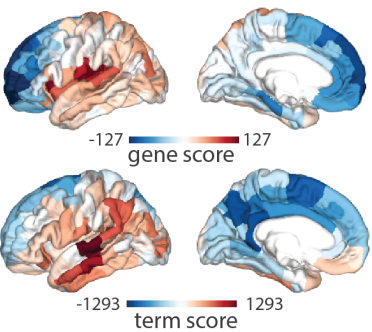
b | spun term association matrix



c | spun gene expression matrix



d | spun term and gene matrices



Supplementary Figure 10. PLS analysis using spun datasets | The empirical PLS results are significant against a spatial autocorrelation-preserving null model (“spin test”). (a) Top: In the original analyses, PLS analysis is applied to gene expression and functional association datasets, yielding a distribution of empirical gene and term scores. Bottom: The null model consists of repeating PLS analysis on the gene expression and term association data, where one dataset has been permuted in a manner that preserves spatial autocorrelation (10 000 repetitions). The resulting null gene (term) score patterns are then correlated with the empirical gene (term) score pattern, resulting in a distribution of correlations for null gene and term scores. A randomly chosen null score pattern is selected for visualization. (b)–(d) Top: an example of a null gene and term score pattern. Bottom: Distributions of the correlation of null and empirical scores. The null model is constructed using (b) spun term functional association data (c) spun gene expression data (d) independently spun gene expression and term functional association data.

air-hunger	disgust	language	phonology	speech (action)
alcohol	emotion	learning	preparation	speech (languag)
amphetamines	estrogen	marijuana	psychiatric medications	SSRIs
anger	execution	memory	reasoning	steroids and hormones
antidepressants	explicit	motion	rest	syntax
antipsychotics	fear	music	sadness	thermoregulation
anxiety	gustation	nicotine	semantics	thirst
attention	happiness	non-steroidal anti-inflammatory drugs	sexuality	time
audition	humour	observation	shape	vision
bladder	hunger	olfaction	sleep	working memory
caffeine	imagination	opioids	social cognition	
capsaicin	inhibition	orthography	soma	
cognition	interoception	pain	somesthesia	
colour	ketamine	pharmacology	space	

Supplementary Table 2. **BrainMap terms** | BainMap terms are organized by behavioural domain. All 66 unique behavioural domain (excluding any undefined domains) used in analyses are shown here.